UNIVERSITÁ DEGLI STUDI
DI MODENA E REGGIO EMILIA

DOTTORATO DI RICERCA IN
MEDICINA MOLECOLARE E RIGENERATIVA
XXXII CICLO

TESI FINALE

Development of a Novel Pharmacokinetic - Pharmacodynamic Preclinical Model for Biodistribution of Mesenchymal Stromal Stem Cells (MSC)

Candidata:
Michela Salvadori

Relatore:
Prof. Massimo Dominici

Correlatrice:
Dr.ssa Alba Murgia

Coordinatore del Corso di Dottorato:
Prof. Michele De Luca

Anno Accademico 2018-2019

To my Family

"Ciò che è difficile attrae,

l'impossibile seduce,

ciò che è complicato spaventa,

ciò che è estremamente complicato innamora."

Paulo Coelho

Index

ABSTRACT (ENG)

Mesenchymal stromal/stem cells (MSC) represent a therapeutic promise in cell and gene therapies. In spite decades of preclinical research and a variety of clinical trial, the lack of established pharmacokinetic (PK) and pharmacodynamic (PD) models are hindering a solid clinical translation of MSC towards patients. Mechanism-based pharmacokinetic-pharmacodynamic (PK-PD) model is a mathematical approach adopted routinely by preclinical pharmacokineticists to simulate the PK-PD profile of a compound candidate to the clinical development and for predicting the clinical dosing regimen. Standardized PK-PD models combined with deepened understanding of MSCs PK and PD could be helpful to improve the therapeutic success of this still promising cell type.

Therefore, starting from a PK-PD model presented by Parekkadan and Milwid in 2010, we address the optimization of a theoretical PK-PD model for MSC biodistribution with the aim to achieve a quantitative approach to be applied in MSC drug development.

MSC pharmacokinetics can be represented by a two-compartment model. Indeed, as represented by Parekkadan and Milwid, MSC concentration was characterized by a decaying exponential kinetic of cellular viability, that on turn affects the time to reach maximal secretion of a molecular mediator, with a short therapeutic window associated with MSC therapy. This model represents a way to address PK-PD model for MSCs, however it does not consider many aspects like the high connection of MSCs with the neighboring environment and the importance of the circulating factors (released by MSCs themselves and other cells) into exerting the PD effect. The Parekkadan and Milwid model is a basic indirect turnover model in which the drug (MSCs) affect simultaneously the pharmacological response (IL-10). However, based on the evidences of MSC injection in a sepsis model LPS-induced (Németh et al. 2010), to which Parekkadan and Milwid referred to, we began to consider a new PK-PD model. After i.v administration MSCs can release prostaglandin-E2 (PGE2) that on turn acts

on PGE2 receptors of activated macrophages inducing the release of interleukin-10 (IL-10) whose function is then to reduce inflammation acting on immune cells. Therefore, MSCs influences PGE2 concentration that on turn rules IL-10 concentration.

While we confirm the two-compartment model to describe the PK of MSCs, we now support that the pharmacokinetic of released factors (PGE2 and IL-10) can be summarized by an unexplored indirect turnover model in which the pharmacological response is not only related to the plasma concentration of MSCs but is dependent also to other factors (PGE2 and IL-10). Basing on the current literature, we evaluated different kind of indirect turnover PK/PD models, trying to simplify the intricate inflammation process that characterize a sepsis model LPS-induced. In vivo data arising from a sepsis mice model are also applied to validate the novel indirect PK-PD models.

ABSTRACT (ITA)

Le cellule mesenchimali stromali / staminali (MSC) rappresentano una promessa terapeutica nelle terapie cellulari e geniche. Nonostante decenni di ricerca preclinica, la mancanza di modelli farmacocinetici (PK) e farmacodinamici (PD) consolidati sta ostacolando la traslazione della dose clinica di MSC nei pazienti. Il modello farmacocinetico-farmacodinamico (PK-PD) basato sul meccanismo è un approccio matematico adottato di routine dagli esperti di farmacocinetica preclinica per simulare il profilo PK-PD di un composto, candidato allo sviluppo clinico e per prevedere il regime di dosaggio clinico. I modelli PK-PD standardizzati combinati con una comprensione approfondita della PK e PD delle MSC, potrebbero essere utili per migliorare il successo terapeutico di questo tipo di cellule.

Pertanto, partendo da un modello PK-PD presentato da Parekkadan e Milwid nel 2010, ci occupiamo dell'ottimizzazione di un modello PK-PD teorico per la biodistribuzione delle MSC con l'obiettivo di raggiungere un approccio quantitativo da applicare nello sviluppo di farmaci a base di MSCs.

La farmacocinetica delle MSC può essere rappresentata da un modello a due compartimenti. Infatti, come rappresentato da Parekkadan e Milwid, la concentrazione di MSC è caratterizzata da una cinetica esponenziale in decadenza della vitalità cellulare, che a sua volta influenza il tempo per raggiungere la massima secrezione di un mediatore molecolare, con una breve finestra terapeutica associata alla terapia MSC. Questo modello rappresenta un modo per affrontare il modello PK-PD per le MSC, tuttavia non considera molti aspetti come l'elevata connessione delle MSCs con l'ambiente circostante e l'importanza dei fattori circolanti (rilasciati dalle MSC stesse e da altre cellule) nell’esercitare un effetto PD.

Il modello basico di Parekkadan e Milwid è un modello indiretto di turnover in cui il farmaco (MSC) influenza direttamente la risposta farmacologica (IL-10). Tuttavia, sulla base delle

prove di iniezione di MSCs in un modello di sepsi indotto da LPS (Németh et al. 2010), a cui si riferivano Parekkadan e Milwid abbiamo iniziato a teorizzare un nuovo modello PK-PD. Dopo la somministrazione endovenosa, le MSC possono rilasciare prostaglandina-E2 (PGE2) che a sua volta agisce sui recettori PGE2 dei macrofagi attivati inducendo il rilascio di interleuchina-10 (IL-10) la cui funzione è quindi quella di ridurre l'infiammazione che agisce sulle cellule immunitarie. Pertanto, le MSCs influenzano la concentrazione di PGE2 che a sua volta regola la concentrazione di IL-10. Mentre confermiamo il modello a due compartimenti per descrivere la PK delle MSC, affermiamo che la farmacocinetica dei fattori rilasciati (PGE2 e IL-10) può essere descritta da un modello indiretto ed ancora inesplorato in cui la risposta farmacologica non è solo correlata alla concentrazione plasmatica di MSCs ma dipende anche da altri fattori (PGE2 e IL-10).

Basandosi sulla letteratura attuale, abbiamo valutato differenti tipi di modelli indiretti PK-PD, che possano semplificare la descrizione del processo infiammatorio che caratterizza la sepsi indotta da LPS. Dati in vivo generati da un modello di sepsi murino sono poi utilizzati per la validazione dei modelli indiretti PK-PD di seguito presentati.

1 INTRODUCTION

Recently, there has been increasing interest in the use of adult stromal progenitors, namely multipotent mesenchymal stromal cells (MSCs), for the development of cell and gene therapies within several biomedical preclinical and clinical applications. MSCs retain promising features both for their ease of use in ex vivo manipulations and for their capacity to generate a therapeutic benefit in early investigations[1,2].

Although the bone marrow has been the main source for MSCs, they have also been isolated from other tissues, including adipose tissue, amniotic fluid, endometrial tissue, dental tissue, umbilical cord, and Wharton's jelly[3,4]. MSCs have been defined as non-haematopoietic progenitors able to self-renew[5], migrate to a site of injury[6,7], differentiate into mesodermal lineages[8], modulate immune response[9,10], and secrete anti-inflammatory molecules[11,12]. These cells can also be easily isolated from different animal species[13] and ex vivo preserved, and they are considered safe because of their low immunogenicity after transplantation[14,15,].

For the last decade, MSCs have been considered as advanced medicinal therapy (AMT), and, therefore, compared to drugs; however, their mechanism of action (MoA) and tissue distribution in several target diseases are still unexplored and not completely understood[16]. Currently, the MoA of MSCs is believed to be associated with their ability to engraft, differentiate, and/or release paracrine signals, but the contribution of each of these properties remain unclear[17,18]. Therefore, the MoA has been described as a complicated network in which MSCs trigger different reactions that also involve other nearby cells with the aim of generating the desired biological function that is then related to a therapeutic effect.

How much the whole cells per se or the released mediators are responsible for the mentioned therapeutic effect is not yet completely known and may also be related to the target disease and the microenvironment. However, it has been observed that a direct injection of biomolecules released by MSCs can provide a benefit above and beyond what is conveyed by

the transplanted cells alone[19,20]. The factors released by MSCs seem to be key players for the beneficial effects after cell transplantation, with the difference being that the implanted cells could constantly release these factors, while an exogenous delivery of MSC-derived biomolecules would require a constant, or at least programmed, delivery, in some manner similar to common pharmaceutical drugs[21]. These still unclear MSC functions and their related bioactive molecules for the intended therapeutic profile pose a challenge to exactly defining the biomarkers linked with an assessment of MSCs' MoA and efficacy[22]. Additionally, it is known that each disease has its own microenvironmental peculiarities (i.e., inflammatory cells, cytokines) that could differentially impact the biological functions of MSCs after in vivo transplantation[23,24,25].

This still obscure but intriguing scenario requires clarification of the basic concepts of MSC-drug development, including the pharmacokinetic (PK) and pharmacodynamic (PD) properties of the cells themselves and their bioactive agents. However, studying PD aspects of MSCs is difficult and results in unclear biomarker definition. Additionally, a substantial barrier to achieve good efficacy is the lack of robust PK data for cells and mediators involved in the biological activity[26]. Increased knowledge of cell distribution after delivery could help to estimate the PK of MSCs and, consequently, define the dosing regimen needed to reach the therapeutic effect. As of January 2019, the number of clinical trials based on MSCs that are publicly available in selected internet resources (www.clinicaltrials.gov) exceeds 800 and many of these studies discuss the possible MoA of MSCs[27,28,29], but data regarding MSC PK and biodistribution are still scarce. For this reason, in this thesis we consider PK aspects of MSCs, we present factors that may influence MSC-based PK studies and we theorise new PK-PD model starting by Parekkadan and Milwid[1,30], the only described model to date.

2 BIODISTRIBUTION OF MSCs IN PRECLINICAL SETTING

Preclinical and clinical investigations have been performed with the aim of investigating MSC tissue distribution, safety, and therapeutic effect to ameliorate pathologic states[31,32]. The following discussion of a series of MSC preclinical studies conducted in the last 30 years delineates fundamental aspects of MSC biodistribution.

MSCs are transplantable via the intravenous route and are trapped in lungs. In 1983, Piersma et al. provided early, pivotal evidence from a murine model of MSC biodistribution after intravenous (i.v.) transplantation of cells tracked by chromosome-marking. Most of the injected cells reached the recipient's bone marrow and remained in situ within 3 months after the transplantation, indicating the ability of injected MSCs to specifically lodge in the host's bone marrow[33]. After those initial findings, many preclinical rodent-based investigations were reported (**Table 1**). In 1995, Pereira gave the first evidence of MSC lung localization following systemic administration. After culture, cells were injected into irradiated mice and detected in the parenchyma of alveoli and bronchi[34]. Subsequently, other studies were performed to better understand this phenomenon and prevent pulmonary entrapment by lung hemodynamic alterations to ultimately increase MSC biodistribution to the target organ[35,36,37,38].

Route of administration and vessel size influence lung trapping. In 2001, Gao et al. infused rat bone marrow MSCs radiolabelled by indium-^{111}oxine through different routes and followed their distribution using whole body scanning and dynamic imaging. The main aim of the study was to compare i.v., intra-arterial (i.a.), and intra-peritoneal (i.p.) infusions. After i.a. and i.v. delivery, the radioactivity was first observed in lungs and then, gradually, in the liver: together, these organs comprised approximately 50% of the infused radioactivity,

confirming the lung as a primary compartment in MSC biodistribution in vivo. In an attempt to bypass lung localization, the same authors introduced sodium nitroprusside as a vasoactive agent, which led to a decrease in lung signal by 15% and an increase in liver distribution, indicating that a simple change in vessel diameter is linked with a different biodistribution pattern, indirectly suggesting a pivotal role of vessel size as a factor contributing to MSC lung localization. In that study, the i.a. and i.v. administrations did not show any significant difference in cell distribution. However, after i.p. infusion, the lung radioactivity was negligible, confirming that an extra-vascular delivery was able to bypass the pulmonary tract[35]. Schrepfer et al. confirmed these findings in a murine model in which cells were monitored by firefly luciferase and green fluorescent dye 5-(and -6)-carboxyfluorescein diacetate succinimidyl ester (CSFE) and tracked post-mortem by histopathology of pulmonary sections. The authors demonstrated that the mean size of the MSCs was larger than the size of the pulmonary capillaries. Thus, large amounts of injected MSCs could be trapped in lung capillaries, thus preventing access to other organs. Further, lung localization could be reduced by a vasodilator[36].

Intrinsic properties and microenvironmental cues affect MSC biodistribution. The findings related to MSC biodistribution seem to be limited by vascular-related issues, such as vessel size and pressure, and by still unclear intrinsic MSC properties, such as cytoskeletal activity, migration capacity, or cell size, that impact specific organ localization. Niybizi et al. reported a graft of green fluorescent protein (GFP)-positive murine MSCs into neonatal mice via a superficial temporal vein. The in vivo MSC tracking was performed by fluorescence microscopy and revealed GFP signal in the lungs, liver, and bone 7 days after infusion. MSCs persisted in the lungs up to 150 days post-transplantation with evidence of tissue-specific differentiation. Engrafted GFP-positive cells were then harvested from bone and infused in

secondary recipients. Curiously, after systemic delivery of these bone-derived MSCs, cells could only be detected in skeletal tissues and not in lung or liver, indicating that intrinsic MSC properties and physiological microenvironmental cues were able to select specific MSC sub-clones associated with a defined biodistribution pattern after systemic delivery in the lack of pathological conditions[37,39].

The role of immunity in MSC biodistribution. At the beginning of 2000, Liechty et al. described the engraftment of human MSCs after in utero transplantation into a fetal sheep with the aim of assessing tissue distribution of human cells into an immunodeficient large animal model. Polymerase chain reaction (PCR) assays, immunohistochemistry, and in situ hybridization were introduced to evaluate the presence and differentiation of MSCs in mesenchymal tissues of the fetal sheep for as long as 13 months. After xenotransplantation, MSCs underwent site-specific differentiation into chondrocytes and in cardiomyocytes, and, even after the development of fetal immunocompetence, MSCs maintained their underlying ability to differentiate in several tissues and maintained their multipotentiality and immunological advantage[40]. On the basis of this data, researchers have investigated the immunology of MSCs and their ability to evade and/or influence the host immune system in relationship with immunosuppression and/or immunoprivilege [41]. The first is due to the MSCs' ability to suppress recipient immune cells[42,43], and the second is based on the negligible expression of the major histocompatibility complex on the surface of MSCs[44,45,46]. Recent data demonstrated an increased level of HLA-DR expression that was irrelevant with regard to MSC capacity to influence lymphocyte proliferation[47]. However, the low MSC engraftment after transplantation may be also related to cell destruction by immune recognition. Zangi et al. suggested that, while luciferase-labelled marrow murine MSCs can retain mild immunosuppressive activity, they do not completely evade the immune system

and induce rejection and memory[48]. Despite that fact, allogeneic MSCs exhibited longer survival than skin fibroblasts, but their survival was shorter than that observed in syngeneic or immune-deficient recipients. Thus, immunogenicity may influence MSC biodistribution in vivo and this must be considered in an accurate selection of the animal model. More recently, authors have suggested that the immunosuppression by MSC may also be exerted after cell destruction opening the field to novel investigations aimed at the deeper understanding on how dying MSC could be immunosuppressive[49].

The role of inflammation and cancer in MSC biodistribution. Inflammatory signals may also impact MSC biodistribution. A paradigmatic example is provided by Wang, who studied the biodistribution of MSCs following both i.a. and i.v. infusions into 2 distinct bone marrow transplantation (BMT) settings: allogeneic and syngeneic BMT[50]. Biodistribution was measured by bioluminescence imaging (BLI) using luciferase-containing MSCs and by 99mTc-scintigraphic imaging. Immunohistochemistry and quantitative real-time PCR were also introduced to support in vivo data. MSC i.a. administration was followed by a wider biodistribution through the body than i.v. delivery, which was primarily characterized by lung localization. Interestingly, MSC migration in the abdomen was more prominent after i.a. delivery within the allogeneic model with gastrointestinal (GI) acute graft-versus-host-disease (GVHD). These data support i.a. delivery of MSCs, further suggesting how microenvironmental cues, such as an inflammatory milieu of GVHD, can influence MSC biodistribution.

In addition, pathological conditions and related factors (i.e., cytokines, chemokines) may influence cell biodistribution with consequences on their therapeutic profile. Lee et al. demonstrated in NOD/SCID mice that i.v.-infused human MSCs ameliorated the outcome of a myocardial infarction model[51]. MSCs were visible by PCR in infarcted hearts starting from

15 minutes after infusion; the visibility peaked 1 day after infusion and then faded. However, a curative effect was observed even after that time due to MSCs trapped in the lung and activated by microenvironmental stimuli to express the anti-inflammatory factor TNF-α-induced protein 6 (TSG-6) that reached myocardial tissue with positive effects. Interestingly, most of the cells were cleared from the circulation in 5 minutes and trapped in the lungs with a half-life of 24 hours. The authors also reported that a small amount (less than 3%) of MSCs reappeared into circulation after lung localization, suggesting a second wave of cells that were then found in other tissues. A comparison of cell distribution 15 minutes after both i.v. and i.a. infusions indicated that the lung was the main organ of distribution; however, after i.a. delivery, more cells could reach the brain, heart, liver, and kidney, which confirmed the findings of Wang[50].

Cancers are also reported as pathological conditions capable of influencing MSC biodistribution[52,53]. A paradigmatic example of this was recently reported by a study in which near-infrared fluorescent nanoparticles (NIR) were used to track the distribution of i.v.-delivered bone marrow MSCs for the treatment of brain tumours. In vivo imaging, histology, and real-time PCR showed that NIR fluorescent labelling revealed a peculiar distribution after systemic injection. MSCs were first detected in lungs within 30 minutes after transplant, and they remained there for up to 4 days; however, the signal gradually decreased in the lungs and increased in the liver and spleen starting from 4 hours after administration and lasting for up to 7 days. The distribution pattern of the migrated MSCs was similar in normal and tumour-bearing mice, although there was a significantly higher presence of labelled MSCs in the brains of the cancer group, with a brain tropism that appeared proportionally inverse to the lung localization[54]. These data indicate that an intravascular distribution of MSCs can reach brain cancer in the presence of blood-brain barrier (BBB) leakage[55]: active or passive homing mechanisms driven by injury and inflammation could explain the migration of the cells across

the BBB. By labelling rat marrow MSCs with intracellular superparamagnetic iron oxide (SPIO), Cheng et al. focused on cell survival and engraftment in a rat model of traumatic brain injury; MSCs were monitored by advanced magnetic resonance imaging (MRI) able to track cells after stereotaxic injection. The authors demonstrated a migration of labelled cells near the lesion area until the third week after injection[56].

While liver has been reported as the target organ in steady-state conditions, liver diseases may influence MSC distribution. Kim used different cell labels (SPIO and metal nanoparticle [MNP]) detected by MRI to monitor MSC implantation, homing, and differentiation in a rat liver cirrhosis model. After 7 days from intrasplenic cell infusion, 3-T MRI tracking and immunohistochemistry revealed a liver accumulation of MSCs around the fibrous septa, suggesting a possible mechanical trapping by portal blood flow as a promoting factor for the liver inlet[57]. Wu used bioluminescence and MRI to track MSCs that internalized PAI/SPION/pDNA. In this case, the combination of bioluminescence and MRI resulted in an efficient and noninvasive in vivo imaging tool to track transplanted cells in a liver injury model. After superior mesenteric vein injection, labelled MSCs were distributed into the liver for up to 10 days, specifically in the sinusoids of periportal areas, underlying the tropism of these cells for diseased tissues that was associated with a therapeutic benefit[58].

The local delivery of MSCs is more appropriate for in situ therapy. Considering the variability in biodistribution after intravascular deliveries and accounting for the fact that a local delivery could be appropriate for defined indications, several research groups focused their attention on local MSC transplantation. Nam et al. introduced a combination of ultrasound and photoacoustic (US/PA) imaging to track and quantify labelled gold nanotraced (Au NTs) MSCs after intra-muscular (i.m.) injection in rat. The US/PA demonstrated that the labelled MSCs can be monitored with high sensitivity and good cell viability over 1 week and

they could be clearly distinguished from other cells and tissue, such as haemoglobin and skin[59]. Years later, Hossain et al. developed a rodent model to monitor i.m.-injected iron oxide-labelled MSCs. MRI and histological analyses were undertaken in rats after MSC injection and showed a high signal that progressively increased over the course of 3 weeks, including adjacent tissue localization[60]. Interestingly, a signal could also be detected in the spleen, indicating that the i.m. delivery could also be associated with broader biodistribution. Despite a large range of reported delivered doses of MSCs (10^4-10^7/animal), key aspects about MSC biodistribution can be summarized (**Table 2**): MSCs are transplantable cells whose biodistribution is influenced by the route of administration, pulmonary vessel size, intrinsic properties, and microenvironmental cues; MSCs can restore tissues by their intrinsic properties and the ability to cross-talk with the pathological microenvironment; the bone marrow has been the most selected source for MSCs, and rodent is the appropriate preclinical model because of its accessibility and the existence of immunodeficient strains; the i.v. route is the most applied preclinical route of administration because it is minimally invasive and because of its putative ability to achieve wide tissue distribution, even in combination with strategies aimed to overcome lung trapping; several in vivo and ex vivo tracking techniques have been combined to describe MSC distribution over time in qualitative and quantitative terms; and the immunogenicity of MSCs allowed preclinical investigations in autologous, allogeneic, and xenogeneic recipients that considered physiological and pathological states.

3 FACTORS INFLUENCING PRECLINICAL MSC BIODISTRIBUTION STUDIES

As stated, MSC biodistribution is influenced by different factors that can be divided in PD- and PK-related factors: the first relates to PD aspects, such as MoA and the recipient biological environment; the second relates to MSC and non-MSC properties affecting PK, such as cell

size, cell source, immunological features and labelling, detection methods, route of administration, and size of the animal model (**Table 3**). Robust investigations of these aspects are lacking, partly due to the difficulty in developing standardized approaches to their study[61,62]. The complexity in this standardization is mostly due to the high variability of PK- and PD-related factors. Reyes recently reported an algorithm for study design to assess MSC biodistribution[62]: this decision tree is based on the results obtained from preclinical studies in different species using diverse delivery routes, cellular labelling, and detection methodologies. Therefore, in this analysis, we sought to further dissect factors involved in the setup of an MSC preclinical biodistribution study. The knowledge of these key factors could lead to better standardization and, above all, more efficient clinical prediction of the clinical dose and efficacy of MSCs (**Table 4 and 5**).

PD-Related Factors

One of the key factors influencing PD is represented by the **MoA and its related therapeutic effect**[17]. MSC therapeutic impact is often driven by different and complex mechanisms, such as the ability of the cell to differentiate in a defined tissue and/or release active substances responsible for efficacy[63]. This complexity can generate uncertain identification and selection of the bioactive substances (MSCs or their released factors) and the efficacy of biomarkers is variable due to many upstream-activated pathways. The knowledge of the MoA ruling pathway is also essential for selection of the MSC delivery route. Indeed, if differentiation is the leading process in MoA, then the cells might be more effective when directly implanted in their site of action; conversely, if secretion is prevalent, then cells can be active even when remotely administrated (i.e., by the i.v. route). Another MoA-dependent gap in understanding is the discrepancy between in vitro and in vivo data: this is particularly true when comparing MSC viability, proliferation, and differentiation capability[64]. This issue can produce a lack of

in vitro-in vivo correlation, which, consequently, generates unpredictable outcomes in terms of clinical efficacy.

A further issue relates to the **MSC therapeutic target**, which can be localized or widely scattered in the body and influences the selection of a local versus systemic route of administration[65]. That, in turn, influences the choice of the most appropriate animal model and adequate tracking methods[66].

Other PD factors to be considered are represented by pathophysiological aspects involved in the often-chaotic background of the target disease and its related microenvironment. The **pathophysiology of the disease** is tightly linked to the type of disease (local or systemic rather than acute or chronic), the patient age (young versus old), and the type of involved cells and the stage of disease (early or advanced). These variables may influence the choice of MSC source, cell doublings, number of injected cells, and route of administration. Also, in this case, the detection and selection of the bioactive substances and efficacy biomarkers can be modified on the basis of the need to treat an acute or chronic state, rather than a young or old patient[67].

The **pathologic microenvironment** to which MSCs are exposed has also become progressively more relevant. The abundance of bystander cells, as well as their recruitments and functions, represent a potent PD-influencing factor[68]. Unfortunately, the interactions between MSCs and the in vivo microenvironment are yet unclear, as are the biomarkers indicative of MSC-based response due to microenvironment regulation[69]. Consequently, there is a need to select and identify bioactive substances and efficacy biomarkers, as well as account for microenvironment effects by in vitro and in vivo correlation assays.

PK-Related Factors

PK-related factors can be subdivided to MSC-related and non-MSC-related factors. The MSC-related PK factors are related to the cells themselves (intrinsic factors), and the non-MSC factors are related to the techniques introduced in a biodistribution study (extrinsic factors).

MSC-related factors. A biodistribution study is dependent on cell-related factors, including the size, the source, the cell doubling, and the immunogenicity of the cells. One of the intrinsic MSC features that influences biodistribution is the **MSC size**, especially in terms of cell diameter. This parameter, dependent on the age and passages in culture[70], can be responsible for trapping in the lung after systemic administration[36]. A diameter between 20 and 24 μm, which is typical of administered cells, dictates that most infused cells remain in the pulmonary region due to their dimension (i.e., they are larger than the size of pulmonary capillaries), and only a low percentage of cells reaches the site of injury[35,36]. Therefore, MSC biodistribution is widely influenced by size, which generates an imbalance between the expected and effective value of cells at the target site and the time needed to reach the target.

It is well known that bone marrow, adipose tissue, and fetal annexes are the most often used **MSC sources** due to similarities (and despite some differences) in morphology, number of isolated cells, and the ability to differentiate in tissues[3]. The choice of MSC tissue source is important both for type of tissue to regenerate and the biological activity required of the cells in the damaged target tissue. For example, it is known that adipose tissue and umbilical cord MSCs give origin to adipogenic[71], chondrogenic[72], and osteogenic[73] lineages. MSC sources can also influence basic cellular features such as surface cellular markers and size[74,75]. To date, there is no preferred source in terms of convenience and quality, but bone marrow is currently the most used[3,31].

The injected MSCs should preferably be derived from **young donors** and undergo **low culture passages** to preserve the proliferation potential and prevent oxidative stress, since increased donor age seems to be correlated with detrimental effects on proliferation and differentiation abilities[31,76,77]. In this regard, the United States Food and Drug Administration (FDA) suggests that propagation of MSCs in vitro should not exceed 5 weeks—the time beyond which these cells are supposed to accumulate mutations[78]. Despite the lower tumorigenic potential of human MSCs compared with rodent MSCs, risk for tumorigenicity after extensive culture should be considered and could impact the accuracy of a biodistribution study[79].

In addition to cell and donor age, **culture conditions** also influence cell performance and senescence, consequently impacting the number of cells administered[80]. For example, a normoxic atmospheric tension (21% O_2), as well as serum starvation and deprivation of growth factors, promotes the generation of free radicals that trigger pathways for apoptosis and premature aging of cells[81]. Additionally, low levels of oxygen increase biological activities involved in the maintenance of stemness, mobilization, homing, and promotion of certain differentiation phenotypes[3]. Interestingly, the introduction of certain growth supplements and/or cytokines can alter immunological profiles of class I and II HLA antigens, which allows for evaluation of the host immune reaction[82].

As described, one of the reasons for a wide diffusion of MSC transplantations is the high degree of safety, as well as the low risk of rejection[1]. Still, it is important to consider possible **donor-related immunogenicity.** A positive outcome of MSC transplantation is presumably due to the cellular immunomodulatory ability that allows the cells to evade the host's immune system through immunosuppressive and immunoprivileged mechanisms[3,49]. However, data demonstrate that MSCs show different distributions when transplanted in an autologous or allogeneic host[48], with allogeneic cells associated with significantly lower survival than syngeneic cells. Although MSC xenogeneic transplantations are characterized by low

immunogenicity, the risk for adverse events is dependent on the host's immune response, which is higher than in autologous or allogeneic settings. Nevertheless, porcine MSCs, one of the most used alternatives to human MSCs, can undergo genetic modifications that further decrease their hypoimmunogenic potential, allowing them to be fully protected from the host immune response[83]. Although this approach retains some promise, so far there have not been reports of clinical xenogeneic MSC transplantation.

Non-MSC-Related Factors

Extrinsic cell-related factors focus on the variables dependent on the setting of a biodistribution study, such as labelling, route of administration, animal models, and detection methods.

The cell labelling and the detection methods are relevant for suitable MSC tracking. Since the beginning of biodistribution studies, scientists followed the fate of MSCs using ex vivo methods, such as real-time PCR and histological assays, which are characterized by low cost, ease of execution, and the ability to be performed after the animal sacrifice. Over time, in vivo imaging has gained favour, permitting an immediate and repeatable surveillance of MSCs and providing high spatial and temporal resolution (**Table 6**)[84]. Even if an ideal imaging method does not exist, it is now possible to select between different techniques, depending on the experimental requirements, including bioluminescence, fluorescence, radio-labelling (positron emission tomography [PET], single photon emission computed tomography [SPECT]), and MRI: each is characterized by different specificity, sensitivity, and type of follow-up. An accurate evaluation of MSC biodistribution should combine both in vivo and ex vivo methods for better interpretation of the results. While imaging provides immediate results[85], ex vivo assays increase the accuracy of outcomes aiming to evaluate sensitivity and

specificity[57]. In vivo methodologies require MSC labelling that can alter MSC migratory ability and viability, which must, therefore, be evaluated before cell delivery[54].

Genetic labelling (e.g., luciferase, β-galactosidase and GFP) requires protocol optimization to obtain high levels of transduction that can delay in vivo administration. This gene labelling is preferred for long-term studies because detection can be maintained after mitosis, although it is potentially associated with genetic instability following transduction. On the contrary, chemical labelling has a shorter duration than genetic labelling because it is diluted in daughter cells after cell division. This, therefore, makes chemical labelling more suitable for short-term follow-up and also accounts for the lack of a robust proliferative attitude of MSCs after in vivo injection[62,86]. In this context, the chemical label transfer from the originally labelled cells to bystander elements or to phagocytes producing false positives must be considered[87,52].

The choice of **animal size** is dependent on the preclinical investigation phases. In early stages, it is preferable to use small animals, while large animals are often required in later stages to mimic the clinical setting; further, in this way, the route of administration must mimic the one intended for clinical trial[62]. This is important since the **route of administration** can influence cell bioavailability. For example, therapeutic targeting can be prevented after a systemic delivery because of the pulmonary first pass[88].

Here, we have described PK and PD factors that influence MSC biodistribution. Since most of the studies have been performed while considering—almost exclusively—PD aspects, we maintain that the PK aspects need attention. Therefore, the next section is dedicated to PK evidence after MSC systemic delivery and to the proposal of a new PK-PD model.

4 PK-PD EVALUATION FOR MSCs

PK describes the time course of drug disposition after administration, and PD focuses on the observed effects resulting from the delivery of a drug[89]. Preclinical PK-PD studies have the aim of establishing a concentration range within a drug to exert its pharmacological effect. In this range, no adverse events should occur and the drug should be considered safe. Consequently, the monitoring of drug concentration is a key step to defining a drug regimen related to both efficacy and safety[90]. In this context, preclinical research on MSCs has underscored the difficulty in exactly knowing the fate and the blood/tissue concentration of the cells after in vivo administration[91]. Indeed, it is difficult to know how many cells die, engraft[92], and differentiate[93] or remain in a steady-state condition. Therefore, defining the cell number responsible for the intended pharmacological effect represents a challenge.

Like cells, small molecules may also undergo variability in their concentrations once they reach systemic circulation. While the PK of a chemical compound is typically dependent on well-characterized properties during drug development, such as the administration route, the physical chemistry (e.g., solubility, stability), the pharmaceutical formulation, and the ADME[94] features (e.g., protein binding, passive/active transports, metabolizing enzymes), MSC biodistribution or PK is influenced by many different factors that are dependent on both the PD and extrinsic and intrinsic MSC-related factors, which complicates a biodistribution study.

Physiologically based pharmacokinetic modelling (PBPK) has been introduced during drug development with the aim of predicting the drug disposition of a candidate compound using preclinical PK data[95]. This mathematical approach is currently recognized by regulatory agencies to simulate the efficacy dose and the related safety margins in humans[96]. In this oversimplified framework, the body is divided into compartments that mimic tissues or fluids

and the time course of drug concentration is described by equations. In particular, in a minimal PBPK model all the highly blood-perfused organs such as heart, lungs, liver, and kidneys are lumped together in one single compartment, while the remained less perfused tissues (e.g fat, muscle, and cerebrospinal fluid) are all included in a second compartment[97]. Unlike physiologically based pharmacokinetic models, the so-called "compartment models or empirical models" are mathematical models, rarely with a physiological significance, but consisting in one or more compartments that are useful to describe the kinetic of the drugs into the body. In the "two-compartment model" the central compartment represents the plasma, while the peripheral compartment is introduced to adjust the shape of the resulting plasma concentration time profile[105].

Attempts to introduce PK models for MSCs are still lacking, and this represents a major limitation. Applying the two-compartment model to small molecules, Parekkadan and Milwid originally proposed a PK concept for MSCs[1]. On the basis of known kinetics data from selected publications, the authors presented a two-compartment model that simplifies the biodistribution of MSCs after i.v. delivery. This model consists of the central (plasma) and the peripheral (tissue) compartments, whose PK parameters are $K_{1,}$ as the constant rate of extravasation between plasma and tissue, and K_2 as the constant rate of intravasation; with R_i and R_c[98] as injection and the clearance rates, respectively (**Figure 1a**). This approach is also based on the following assumptions: **a**. MSCs looks like inert and spherical (d=20 μm) particles that have no interaction with the host; **b**. the cells contain a fixed concentration of molecules that is equivalent to 100% of the bioactivity; **c**. the transport of the single molecule from the cell directly into the bloodstream is not rate limiting; **d**. the therapeutic index is directly proportional to the serum concentration profile of the molecules secreted by the MSCs.

In a *theoretical engraftment*, where it is assumed that, after MSC transplantation, nearly 100% of the cells remain viable and effective after infusion, an apparent activity (the unit activity per cell multiplied by the number of cells after injection) is maintained over the time course and long-term therapeutic action is guaranteed (**Figure 1b**). However, based on experimental evidence of MSC i.v. delivery, a better term is *apparent engraftment* (**Figure 1C**).

An apparent engraftment is characterized by a quick infusion of a dose of drug (R_i) in the bloodstream, so that R_i is considered negligible and the plasma concentration (C_p) of the drug is 1 (C_p=1). The clearance rate (R_c) and the rate of intravasation (K_2) are higher than the rate of extravasation (K_1). Consequently, the exchange between the 2 compartments is practically null and the MSCs stay in the central compartment. Parekkadan and Milwid represent the apparent engraftment as in figure 1C: the MSCs show a rapid decline of cellular viability[48,51], which, in turn, affects the time to reach maximal secretion of a molecular mediator (apparent activity) with a short therapeutic window associated with MSC therapy. Consequently, according to this model, the therapeutic activity would be maintained for 24 hours and, for extended efficacy, multiple administrations with a range of 24 hours would be necessary. This may need to be addressed by comparative clinical trials in which cells are delivered daily versus weekly, as is currently done for GVHD treatment[99].

While the model by Parekkadan and Milwid still represents a way to address a basal PK-PD[100] model for MSCs, many aspects need to be considered to carefully establish a model able to make clinical predictions about MSCs, their doses, and their schedules in vivo. Although i.v. administration is the route most applied in preclinical and early clinical studies, it may not be the best route to allow MSCs to reach the target organs[57]. Therefore, we can suppose that, by changing the route of administration, PK parameters of the two-compartment model will not be completely applicable, possibly due to a lower clearance, a higher apparent activity, and a shift of the model that may become closer to that of the theoretical engraftment.

Moreover, undefined mechanisms of action and the high connection of MSCs within the neighbouring environment make these cells non-inert particles whose biological activity can be dependent on many bioactive circulating factors that are released (directly or indirectly) by injected MSCs or by other cells (i.e., MSC-activated)[101,102]. Thus, the bioactive substances to be included in the PK-PD model are not only limited to the MSC number but are also related to either the levels of soluble factors constitutively released by the cells themselves or to substances that may be released by MSCs after in vivo infusion due to microenvironment conditioning. This aspect adds complexity that needs to be addressed by new models and the high variability of biomarkers detected needs to be considered in a novel PK-PD prediction. Consequently, the final apparent activity will be the result of all the different biomarkers acting within a defined time frame and also involving bystander cells.

Therefore, we began to reason a new PK-PD model based on the described considerations (**Figure 2**). This model, defined as ***two-functional-compartments***, is based on the fact that, after infusion, MSCs can release molecules (cell-related biomarkers) capable of functionally influencing bystander cells (i.e., macrophages) that, in turn, can release bioactive substances that we propose as efficacy biomarkers of the desired therapeutic effect. While the cell-related biomarkers are responsible for the PK activity of the MSCs, the efficacy biomarkers reveal the PD activity. In addition, considering that microenvironment cues may influence MSC-related biomarker release, we should consider that the effect of MSCs on bystander cells could be temporally shifted, impacting the PD of infused cells. To provide an initial justification for this model, we report the original Németh et al. study, which aimed to attenuate sepsis after i.v. MSC administration[30]. The authors describe that MSCs can release prostaglandin-E2 (PGE2) (as a cell-related biomarker) that acts on PGE2 receptors of activated macrophages (PGE2 and E4 receptors), which induces the release of interleukin (IL)-10 (an efficacy biomarker) whose function is then to reduce inflammation by acting on immune cells. Thus,

we represent the cell-related biomarkers, MSCs and PGE2, in the first two-dimensional graphs of **Figure 2** and the efficacy biomarker IL-10 in the second graph. Much of these data supporting this concept have been reported[103]. In the definition of this proposed two-functional-compartments model, we also consider that several complex factors may affect the outcome of MSC biodistribution: in particular, factors involved in the MoA (PD factors) and factors related to the cells themselves (PK-related factors), as described in the previous paragraph.

5 PROPOSED MODELS FOR MSCs EFFECT IN MURINE SEPSIS

The two-functional-compartments model (**Figure 2**) related to Németh study can be further evolved in a turnover model. Turnover concept is applicable to the majority of endogenous compounds (e.g hormones, proteins, enzymes), whose homeostasis is an equilibrium between their production (synthesis, secretion) and loss (catabolism, filtration). In turn, these processes are represented by parameters (e.g biological half-lives) that can be described by mathematical equations[98]. In a basic turnover model (**Figure 3**) we define K_{Syn} and K_{Deg} as synthesis and degradation parameters of R, the response of a specific substance, that is the concentration of a biomarker (e.g a cytokine) itself over the time. In order to extrapolate R, $\frac{dR}{dt} = K_{Syn} - K_{Deg} *R$, a change in K_{Syn} or K_{Deg} (due by the promoting or inhibitory effect of the drug A), affects R that can be written as $\frac{dR}{dt} = K_{Syn}*f(DrugA) - K_{Deg} *R$ and or as $\frac{dR}{dt} = K_{Syn} - K_{Deg} *f(DrugA)*R$.. In a baseline condition, in absence of any kind of stimulus $R_0 = \frac{KSyn}{KDeg}$.

Therefore, we can use these equations to describe the turnover of the cytokines involved in the sepsis model, represented in **Figure 2a**. The molecular pathway described by Németh et al. in a sepsis state, is a turnover indirect model in which the pharmacological response

consequently to MSC injection, takes time to develop and it is not directly related to the MSC concentration. MSCs triggers a turnover mechanism characterized by the response of mediators and bystander cells such as PGE2, activated macrophages and IL-10 whose function is to reduce inflammation acting on immune cells. Therefore, the setting-up of a PK-PD model of anti-inflammatory MSC effect in the sepsis-model, requires the pharmacokinetic of MSCs, LPS and then, with a drop-down effect, PGE2, activated macrophages, IL-10 and TNF-α response. Going over the literature, we speculate three indirect turnover PK-PD models discerning by different levels of complexity.

In the Model I, the drug represented by the MSCs, modulates the response following the differential equations reported previously above, where $\frac{dR}{dt}$ is correlated to the MSCs concentration that in turn can modulate K_{Syn} and K_{Deg}. LPS is instead constant and not included in the modelling[104] (**Figure 4a**).

Other literature studies describe the pharmacokinetic of the challenger, in our case LPS. In these indirect Model II, the response of a biomarker $\frac{dR}{dt}$ is a function of LPS and DrugA, as reported in **Figure 4b**, here, the time courses of the drug (MSCs) and of the challenger (LPS) are included. In this regard, Gabrielsson et al.[105] proposed a so called "transduction PK-PD model" in which the time courses of a test drug (Anakinra), a challenger (IL-β) and cytokine (IL-6) were evaluated in order to investigate the cytokine response following IL-β challenge, with or without drug intervention. In absence of the drug, the time course of the cytokine IL-6 was induced by IL-β challenge, therefore IL-6 response was as follows: $\frac{(dIL-6)}{dt}$ = K_{Syn} *f(LPS) – K_{Deg} *R. In presence of Anakinra, IL-6 concentration was subjected to inhibition, therefore $\frac{(dIL-6)}{dt}$ = K_{Syn} *f(LPS) *f(Drug) – K_{Deg} *R or K_{Syn} *f(LPS) – K_{Deg} *f(Drug) *R, if the drug affected K_{Syn} or K_{Deg}.

Finally, we also present a Model III (**Figure 4c**) that can be defined a high-order model, developed to predict the pro- and anti-inflammatory responses. This model includes biological complexity predicting the dynamics of individual cytokines, considering the network of the molecular pathway. This is the model that looks alike closer to the reality, un fact it takes into consideration the cytokines, the inflammatory cells (activated monocytes and macrophages) and their feedback connections[106].

With the aim to validate a PK-PD model in a sepsis murine context LPS-induced, we have collected plasma samples in order to quantify PK and PD biomarkers (including PGE2, IL-10 and TNF-α), following i.p administration of LPS. In a next study, the administration of bone marrow derived-mesenchymal stromal cells will be crucial both for investigating the relationship between the pharmacokinetic and the pharmacodynamic of MSCs in the same sepsis murine model and for validating a computational PK-PD model.

6 MATERIALS AND METHODS

6.1 Experimental procedures for bone marrow derived mesenchymal stem/stromal cells isolation and culture

Mice were housed in a specific pathogen-free facility (Biostab, UNIMORE) and fed a diet without chlorophyll. All animal procedures were performed under license from the Department of Medical and Surgical Sciences for Children & Adults, University Hospital of Modena and Reggio Emilia and approved by the local Ethics Committee. 6-week-old SKH1 mice will were shipped to Dr Phinney Lab (Jupiter, Florida) in order to isolate BM-MSC.

6-week-old SKH1 mice were euthanized by exposure to CO_2 and the carcass were then rinsed with 70% ethanol. The hind limbs were dissected in a sterile cabinet and stored on ice in PBS supplemented with antibiotic (1× penicillin/streptomycin) while awaiting further dissection. Muscle and connective tissue were removed from the femur and the tibia. Extrusion of the bone marrow were performed in a standard biosafety cabinet using proper sterile technique. The ends of the tibia and femur were cut just below the end of the marrow cavity, which is evident by the transition from a red to white coloration in the bone, using a pair of sharp scissors. A 22-gauge needle attached to a 10 cc syringe containing complete medium were then inserted into the spongy bone. The marrow plug will be flushed from the bone with 0.5 ml of complete medium and collected in a 50 ml conical tube on ice. Marrow plugs were dissociated into a single cell suspension by repeated passage (3×) through an 18-gauge needle attached to a 30 ml syringe. The cell suspension was then filtered through a 70 μm strainer to remove any bone spicules. Cell yield and viability were determined by trypan blue. Cells were seeded at a density of 2×10^6 cells/mL and incubated in a humidified incubator at 37°C with 5 % CO_2. After 72 hours, the non-adherent cells that accumulate on the surface of the dish were re-suspended by gentle swirling, aspirated, and replaced with complete medium. The primary cultures were approximately 80% confluent in one week or 10 days. Media were

replaced every 3-4 days. All cell manipulations were done using an airtight, oxygen-controlled chamber in 5% oxygen.

For subculture, plates were washed with PBS 1x and incubated for approximately 5 min at 37°C with 0.25 % trypsin/0.02 % EDTA. A small amount of medium supplemented with FBS (0.5 ml) were added to inactivate the trypsin. Cells were centrifuged at 300xg for 10 min at room temperature and suspended in α-MEM supplemented with 20% defined FBS (heat inactivated) and 10 μg/mL ciprofloxacin. At culture passage 1(P1) cells were seeded at a density of 1×10^4 cells/cm^2. Starting from P2 the cells were seeded at a density of 5×10^3 cells/cm^2.In order to fractionate MSCs from hematopoietic lineages in plastic adherent cultures the immunodepletion by Dynabeads® conjugated with CD11b, CD34, and CD45 antibodies were performed as reported[107].

6.2 Mice BM-MSC characterization by FACS

To assess the immunophenotype, at culture passage 1 (P1) the adherent cells were harvested for surface antigen analysis. BM-MSC were detached from plastic support with 0.25% trypsin/0.02 % EDTA, counted, and aliquoted in FACS analyses polypropylene tubes (0.5–1x10^6 cells/tube). BM-MSC were incubated in blocking buffer (100 μL each 0.5–1x10^6 cells) containing Dulbecco's Modified Eagle's Medium, 10% FBS, and 0.1 M sodium azide and human immunoglobulin γ and incubated for 20 minutes on ice.

The samples were washed in PBS 1x and re-suspended in PBS with 0.5% bovine serum albumin and stained on ice and in the dark for 30 minutes with the following rat anti-mouse dye-conjugated monoclonal antibodies: APC anti-CD45 and BB515 anti-SCA1. In all the experiments, the corresponding isotype-matched antibodies were used as negative controls. Cells were stained with 7AAD in order to select only the viable cells. Data were collected using a FACS Aria III flow cytometer and analysed on FACS Diva software.

6.3 Mice BM-MSC labelling by DiR

In order to identify the BM-MSC biodistribution, at culture passage 2 (P2) the adherent cells were washed with PBS (3 times), detached from plastic support with 0.25 % trypsin/0.02 % EDTA and centrifuged at 300xg for 10 min. Then, the cells were incubated in 3.5µg/mL DiR (in PBS) for 30 min at 37°C. At the end of incubation, the labelled cells were spun down at 1000rpm, for 3 min at 4°C, resulting in a blue pellet. In order to remove free dye cells, the pellets were washed 2x in PBS (cells were centrifuged after each wash: 1000rpm, 3min 4°C). After washes, the cells were eluted into PBS. Cell suspensions were counted and 1milion of labelled (DiR+) or un-labelled (DiR-) cells in 200 µL of PBS were injected i.p. in the mice.

6.4 Sepsis animal model

For the purpose of this pilot study, male SKH1 mice aged between 6-8 weeks were introduced in the study. Animals were grouped of 4-5 in polypropylene cages with wood chip bedding and environmental enrichment (shredded paper and cardboard tubes). All injections were prepared fresh on the treatment day and given intraperitoneal (i.p) in a final injection volume of 100 µl. Controls (group1, n =7) received sterile i.p injection of phosphate buffered saline (PBS, pH 7.4) (n=7), while lipopolysaccharide was made up to 40 µg/mouse (group 2, n=7) or 10 µg/mouse in (group 3, n=7)[108]. LPS was diluted in a final volume of 100 µl PBS pH 7.4. Animals were sacrificed at 6 and 24 hours. Whole blood was collected into commercially available heparin-treated tube. Cells were removed from plasma by centrifugation for 15 minutes at 1,000x g using a refrigerated centrifuge. The resulting supernatant was designated plasma. Plasma was transferred into a clean polypropylene tube. The samples were maintained at 2–8°C while handling. If the plasma were not analysed immediately, the plasma was apportioned into aliquots, stored, and transported at –80°C for the analysis. It is important to avoid freeze-thaw cycles.

Treatment groups:

(A) LOW DOSE LPS: 10 µg/mouse by i.p (8 µl stock solution 1250 µg/ml) (time points = 1 h (S1), 6 h (T2), 24 h (T1) n = 14)

(B) HIGH DOSE LPS: 40 µg/mouse by i.p (32 µl stock solution 1250 µg/ml) (time points = 1 h (S1), 6 h (T2), 24 h (T1), n = 14)

(C) CONTROL: 100 µl PBS (vehicle). (the animals were sacrificed at 6 h, n = 7)

Notes: S1= group 1 n=7, plasma samples collected at 1 hour after LPS injection; T2= group 2 n=7, plasma samples collected at sacrifice, 6 hours after LPS injection; T1= group 1 n=7, plasma samples collected at sacrifice, 24 hours after LPS injection. Total of 35 animals, 49 plasma samples collected.

6.5 Cytokines measurement in murine plasma

PGE2 and cytokines (IL-6, IL-10, IL-13, IL-2, TNF-α, MIP1α, MIP1β, GMCSF, TNF-α, MCP-1, IL-β, IL-27, MIP2, RANTES, KC, IL-5, EOTAXIN, IP-10, IFN-γ.) were quantified with ELISA kit at each time point (kit code KGE004B and LXSAMSM-21 respectively, all from R&D System, Minneapolis, MN, USA). In particular, in euthanized mouse a cardiac puncture was performed to isolate 500 µL of total blood. The tubes containing total blood and EDTA were centrifuged to isolate the plasma. Plasma samples were stored at –80°C until assayed. The results were expressed in pg/ml represented as mean values ± SD of the mean. Statistical analysis was performed using Graph Pad Prism 8.3 software (GraphPad Software, La Jolla, CA). The three arithmetic averages obtained by each sample of a group were analysed by using two-way ANOVA (*$p < 0.05$; ****$p < 0.0005$). All data were shown as mean ± SD.

6.6 Proposed model for MSC sepsis model

Basing on literature we proposed theoretical PK-PD models. Considering that in our murine disease model the factors involved were LPS, MSCs and cytokines, we developed a type II model to connect LPS, MSCs and cytokines, as reported (**Figure 5a**).

Observed data arising from in vivo study were plotted for each cytokine concentration versus simulated data ruled by differential equations of the supposed model. If the observed and the simulated curves fitted, as indicated by the ordinary least squared values or residual analysis[105], the proposed model was applied to describe the PK-PD relationship of our sepsis model.

By referring to Gabrielsson[105], we extended differential equations for the description of the relationship between LPS, MSCs and cytokines (**Figure 5b**). MSC and LPS equations described the concentration of MSC and LPS respectively, over the time course. Cytokine equations described the time course of the cytokines that were in turn influenced by K_{Syn} and K_{Deg} of the cytokines themselves, the maximum cytokine concentration and the 50% of the maximum concentration of cytokine induced by LPS or MSCs, and the concentration itself of LPS or MSC. Considering an i.p route of administration, the MSCs and LPS kinetics followed the rules of a two compartments model, where the dose was the first compartment and the second, the central (plasma) compartment (**Figure 5c**). The dose compartment kinetic rule or the rate of absorption of the dose was: $\frac{dA}{dt}$ = dose – Ka*A, where A was the amount of the dose remained to be absorbed, Ka was the absorption constant that drives the MSCs or LPS from the dose to the central compartment. The kinetic into the plasma compartment was described by this equation: V * $\frac{dC}{dt}$ = Ka*A – Cl*C, where Cl was the clearance from plasma compartment and C the concentration of LPS or MSCs. Instead, the cytokines followed equations in which the stimulus or the inhibitory effect induced by MSCs and/or LPS were

considered and so reported, $1 + \frac{Smax*C^n}{EC_{50}^n+C^n}$ and $1 - \frac{Imax*C^n}{EC_{50}^n+C^n}$, I and S are related to inhibitor or stimulus effect of LPS or MSCs and n is a Hill coefficient. Therefore, $\frac{dR}{dt}$ = K_{syn} *$(1 + \frac{Smax*C^n}{EC_{50}^n+C^n}$ * (1- $\frac{Imax*C^n}{EC_{50}^n+C^n}$)) -$K_{deg}$ * [R].

7 RESULTS

7.1 Mice BM-MSC expansion and characterization by FACS

BM-MSCs cells isolated by 6-week-old SKH1 mice in collaboration with Dr Phinney Lab (Jupiter, Florida) to Department of Medical and Surgical Sciences for Children & Adults (Modena), were thawed and plated in α-MEM + GlutaMAX supplemeted with 5% human platelet lysate (hPL). Cells were incubated in a humidified incubator at 37°C in 5% oxygen for 3 days. At the end of the third day, at passage (P) 1 the BM-MSCs showed a fibroblast-like morphology typical of murine MSCs, but no proliferation was observed (**Figure 6**). Murine MSCs were detached and analysed by FACS. (**Figure 7**). BM-MSCs were detected basing on the size (FSC-A) versus granularity (SSC-A) and SSC-A versus the absence of the apoptotic marker surface 7AAD (**Figure 7a and 7b**). 95% of the BM-MSCs resulted alive ($7AAD^-$). Moreover, the cells with the isotype CD45 and SCA1 were checked in order to distinguish between the hematopoietic ($CD45^+$) and mesenchymal stromal ($SCA1^+$) lineages (**Figure 7c and 7d**). SCA1 was indeed the marker surface of MSCs able to differentiate to osteocyte, adipocyte and chondrocyte lineages[109]. Murine MSCs resulted CD45 negative and positive for SCA1.

7.2 Mice BM-MSC labelling by DiR

BM-MSC cells of culture P2 were detached, centrifuged, counted and stained with 8.2 µM DiR. BM-MSCs ($1x10^6$) were labelled and injected i.p ($1x10^6$ in 200 µl PBS) in mice. Negative controls (PBS only injected) were also included. After both 1 hour and 24 hours from the injection, MSC-treated and control negative mice were visualized by IVIS imaging (**Figure 8**). After 1 hour, no signal was detected, however after 24 hours the fluorescence was visibly marked in the abdominal part. In particular, the spleen was strongly positive.

7.3 Cytokines measurement in plasma samples

PGE2 and cytokines were quantified in SKH1 murine plasma (**Figure 9**) obtained after sacrifice at 1 h, 6 h and 24 h of control, low and high dose of LPS. In the measurement of PGE2, the control group showed 18012.1 pg/ml, while the 10 μg and 40 μg LPS-treated groups did not show any significant increase at each concentration of LPS administered. IL-6, TNF-α, GM-CSF, MCP-1, MIP-1β, IL-4, IL-1β, IL-10, IL-17α, MIP-1α, IL-27 levels showed a marked and highly significant response in comparison to the control group at 1 hour. Particularly, IL-6, MCP-1 and MIP1-β reach marked plasma levels between 20,000-50,000 pg/ml with 10 μg of LPS. Interestingly, MIP-2, RANTES, EOTAXIN, IFN-γ, KC, IL-5 and IP-10 increased later in plasma, showing a concentration peak at 6 hours. No relevant amount of mediators at 24 hours, except for EOTAXIN and KC chemokines, could be detected. On contrary, IL-12p70 significantly decreased at 1, 6 and 24 hours at the administrated dose of 10 and 40 μg LPS. IL-13 and IL-2 showed levels below the quantitation limit (BLOQ).

7.4 Proposed model for MSC sepsis model

To set-up the PK-PD Model II we began to refer to LPS and MSC experimental data from literature. Specifically, for LPS we simulated a dose of 10 μg and 40 μg considering the kinetic profile of LPS in murine plasma after i.p injection measured by Barros et al.[110]. Moreover, for MSC we proposed the kinetic profile described by Shim et al.[111], simulating the MSC pharmacokinetic after the administration of $1x10^6$ MSCs per mouse by i.p. In **Figure 10**, we reported the results obtained by the computational PK-PD Model II. In **a,** the kinetic profiles of TNF-α, IL-6, IL-10 and PGE2 were expressed as observed and simulated, in vehicle, high dose and low dose of LPS groups. In **b,** the cytokine kinetic profiles were simulated considering the MSC effect. Observed and simulated data seem nearly overlap when MSC effect was not considered (**Figure 10a**).

8 DISCUSSION AND CONCLUSION

This thesis focuses on MSC biodistribution, addressing the PK and PD aspects of these intriguing stromal progenitors originally reported in the 1960[112].

Considering their safety, MSCs have been introduced into clinical practice for a variety of severe and/or rare pathologic conditions when standard approaches have limitations or are no longer effective[113]. Despite the growing applications of MSCs in trials, much still needs to be addressed regarding their biodistribution, especially since clinical success of an MSC-based product should require preclinical research with appropriate PK-PD investigations in early phases of development to better understand MSC functions and increase their efficacy in patients. In this way, the progression of MSC-based therapy towards improved clinical development could be expedited and early interruptions or unexpected results in later phases could be avoided. Currently, of the 800 clinical studies on MSCs, less than 5% are phase III trials (source: www.clinicaltrials.gov; searching with key words: MSCs, mesenchymal stem cells, mesenchymal stromal cells) and only 10 MSC-based products have been granted market authorization so far, which may also suggests that the lack of PK-PD studies might impact clinical development[114]. In practice, a translation preclinical-clinical PK-PD model is not considered by the regulatory agencies for establishing the optimal dosage of MSCs. In fact, FDA guidelines[115] recommend to provide preclinical proof of concept and toxicological studies that include the determination of the pharmacologically effective dose range; the optimization of the route of administration with confirmation that the product reaches the target anatomic site; the optimization of the timing of administration relative to disease onset and finally the characterization of the putative mechanism of action[116]. Robust results from preclinical animal research and novel 3R-respecting in vitro investigations could provide MSC PK and PD data that are useful for clinical dose planning in the same way that it has

been applied for biologics and small molecules[117]. For this reason, we focused first on key PK- and PD-related factors and their associated variables that may pave the way for standardization in MSC biodistribution research, and successively on a PK-PD model.

The proposal of a PK-PD model[118] represents a promising challenge to overcome the preclinical-clinical gap in which the based-MSCs therapeutic strategy may collapse. For this reason, we wanted to introduce several PK-PD models that simulate the relationship between the pharmacokinetic of the drug (MSCs) and the pharmacodynamic effect of the cytokines in LPS-induced sepsis model, presenting different levels of complexity. In fact in a simple Model I, only MSC turnover is considered having an impact on the cytokine release and persistence. However, the involvement of LPS and MSC on cytokine response is considered in a Model II and also in a more complicating Model III, in which many feedbacks are inserted to mimic a more realistic molecular pathway. Simulated PK-PD model II of preliminary in vivo sepsis model results show that the Model II seems to better highlight that the observed data show a good fitting with the simulation driven by the Model II differential equations **(Figure 10a).** Next in vivo studies will be necessary to confirm whether the proposed PK-PD model could predict the cytokine kinetic profiles after MSC administration in a sepsis LPS-induced mice model **(Figure 10 b).** Moreover**,** we retain that an accurate validation of the PK-PD Model II, would require the sample plasma analysis obtained by at least three LPS and MSCs dose treatments in a long time course, so that a good correlation between the predicted and observed data generated by different MSCs and LPS doses, allow us to adopt the PK-PD model to simulate PK-PD effect following different LPS and MSCs murine administration. Nevertheless, the implementation of a human PBPK model and literature clinical data[119], could support us to predict the human efficacy MSC dose to adopt in a sepsis condition.

Therefore, considering our PK-PD sepsis model, a good preclinical-clinical translation would require (a) to clarify the PK-PD effect by collecting in vivo preclinical PK MSC data and the

respective cytokine levels; (b) the development of a PBPK modelling to characterize the in vivo kinetics of MSCs in the animal model; and (c) the PBPK model calibration for interspecies scaling of the PK-PD effect. Considering our strategy, we can assert that the collection of murine MSC biodistribution data will be crucial for the PBPK advance. Once the PBPK model simulation will be established, a comparison between observed experimental and predicted data will be performed for model validation. Additionally, the comparison of II and III Models could be of utmost importance to investigate which of the two computational models may be more suitable to dissect the complicated connections established in the inflammatory state of LPS-induced mouse model.

Looking at the investigation of the cell-related and efficacy biomarkers, the in vivo pivotal LPS-mice study provided important information about the sepsis condition. PGE2 plasma levels did not show significant increase after LPS stimulation, although a mild release was detected at 1 hour at both LPS doses. This result agrees with in vivo LPS-induced mouse acute liver injury model, in which PGE2 level in LPS group is nearly close to the control group after 12 hours from the administration[120]. On the opposite, in vitro results of murine RAW264.7 macrophages culture treated with LPS resulted in 3-fold increase of PGE2 levels at 3 hours after LPS, compared with untreated culture. We can suppose that the different results need to be searched in the dissimilarity between in vitro and in vivo experimental methods. In fact in the first case, LPS treatment promotes the direct activation of macrophage culture to induce PGE2 secretion; in the second one, i.p administration of LPS spread an inflammatory state that involves many immune cells and cytokines[121]. Plasma cytokines analysis showed that the prominent increase of IL-6, TNF-α and IL-10 levels (together with other inflammatory mediators) at 1 hour (above all at 10 μg), were a clear early inflammatory signal. This was also supported by Hao[122] sepsis LPS mice model, where IL-6, IL-1β, TNF-α showed a peak concentration until 3 hours before to decay; moreover Németh[30] reported that IL-10 reached

a peak concentration at 6 hours after cecal ligation induction. Particularly, IL-6 and MCP-1 reached the highest plasma levels at 1 hour after LPS 10 µg. It is in fact well known that IL-6 and TNF-α are abundantly secreted by monocytes and macrophages after the interaction of LPS with their membrane receptor CD14. This activation provides the background for the septic pathophysiology induced by LPS[123]. Although the IL-4 cytokine is still high at 6 hour both at high and low dose, most of the early mediators show a drop-off at this time point, making way at the chemokines such as MIP-2, RANTES, EOTAXIN, KC and the cytokines IFN-γ, IL-5 and IP-10. Therefore, we can speculate that after a first immediate release of a cytokine wave at 1 hour, the immune system at 6 hours is stimulating the recruitment of different types of leukocytes (chemotaxis) to the site of inflammation, as if the chemokines themselves had an essential role in leading both the immune cell trafficking and then the transition step between the innate immune and the adaptative cells[124]. As proof of concept, the persistent plasma levels of EOTAXIN and KC at 24 hours, chemokines usually involved into leukocyte migration and into the onset of inflammatory disorders, seem to indicate a continuum in the inflammation process promoted by LPS, in particular at 40 µg 24 hours, however the BLOQ levels of IL-13 that is mainly produced by the adaptive immunity cells Th2 cells[125]evidences that the adaptive immune response is not yet noticeable. Therefore we can affirm that we induced a primary immune response after 10 µg and 40 µg of LPS administration and the innate immune cells are prevalent, as expected[126].

In conclusion, reproducing a sepsis murine model LPS-induced, we have provided preliminary data for the validation of a PK-PD MSC model that underscores the importance of PK and PD for the success of MSC-based therapies.

FIGURES

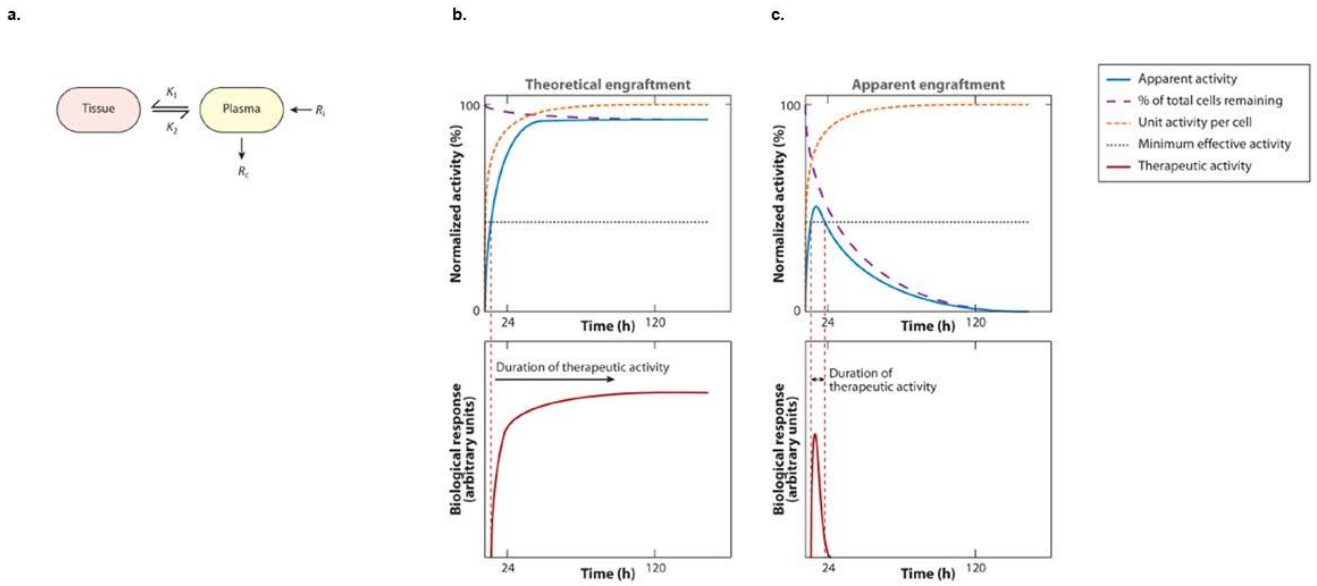

Figure 1. Parekkadan and Milwid pharmacokinetic analysis of MSCs. a. Two-compartment pharmacokinetic model of MSCs after intravenous (i.v.) delivery. R_i, injection rate; R_c, clearance rate; K_1, rate of extravasation; K_2, rate of intravasation. **b**. Theoretical engraftment of MSCs with assumption of 100% cellular viability and activity over time. **c**. Apparent engraftment of MSCs with a decaying retention of 24 hours. The apparent activity is considered to be the product of the unit activity per cell and the number of cells remaining after injection (Parekkadan et al. 2010).

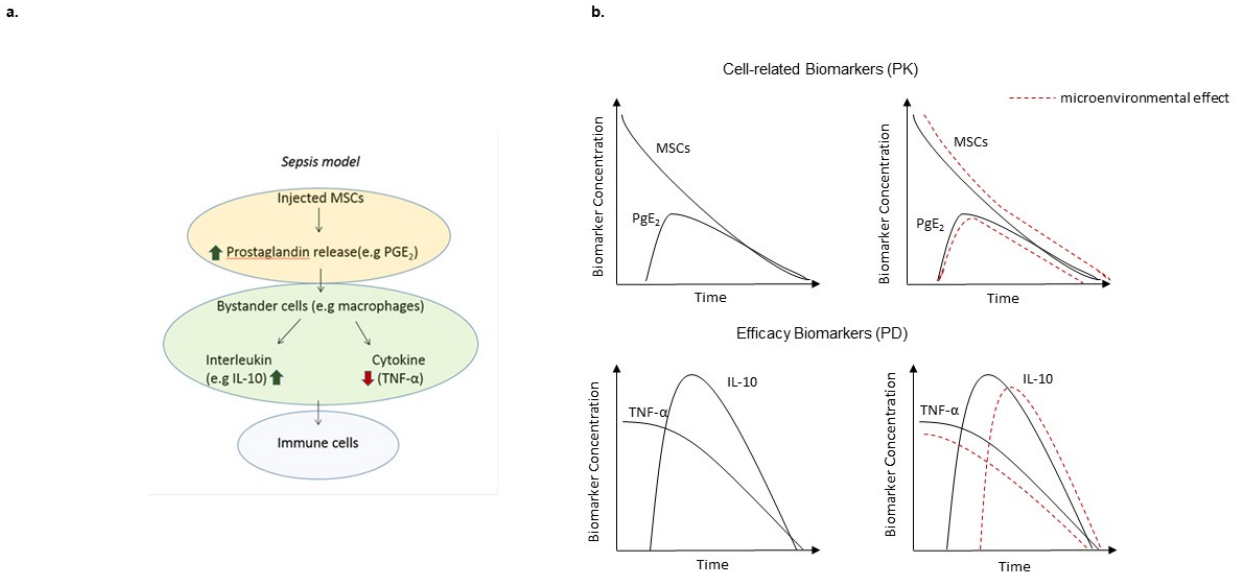

Figure 2. Two-functional-compartments PK-PD model in sepsis. **a**. Multipotent mesenchymal stromal/stem cells (MSCs) are challenged in a sepsis model causing prostaglandin-E2 (PGE2) release that, in turn, acts on PGE2 receptors on macrophages. The macrophage receptor binding is responsible for the increase in interleukin (IL)-10 production and a reduction in serum tumour necrosis factor (TNF) -α. The molecular pathway was described by Németh et al. 2009. **b**. The two-functional-compartments PK-PD model. The PK biomarkers are the MSCs and their secreted molecules leading to the PD effect. The PD biomarkers are the cytokines as markers of the therapeutic activity.

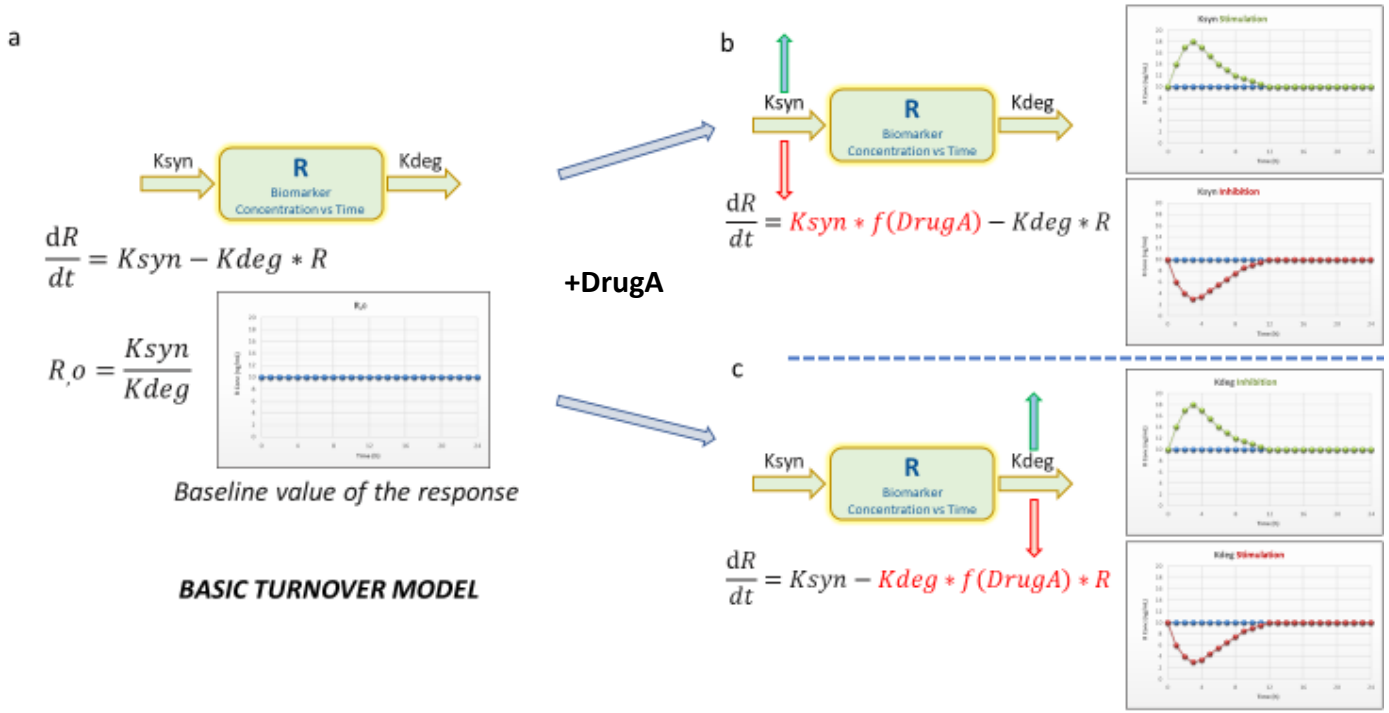

Figure 3. **Basic principles of turnover model**. In a turnover model, R is the amount of a specific substance (e.g a cytokine), secreted or synthesized per unit time, $\frac{dR}{dt}$ = K_{Syn} – K_{Deg} *R. **a.** In a baseline condition in absence of any kind of stimulus, the rate of change of R is equal to zero and R_0 = $\frac{KSyn}{KDeg}$. **b**. The drug A can affect R in K_{Syn}, resulting in $\frac{dR}{dt}$ = K_{Syn} * f(DrugA) – K_{Deg} *R; **c.** The drug A can affect R in K_{Deg}, resulting in $\frac{dR}{dt}$ = K_{Syn}– K_{Deg} *f(DrugA) *R.

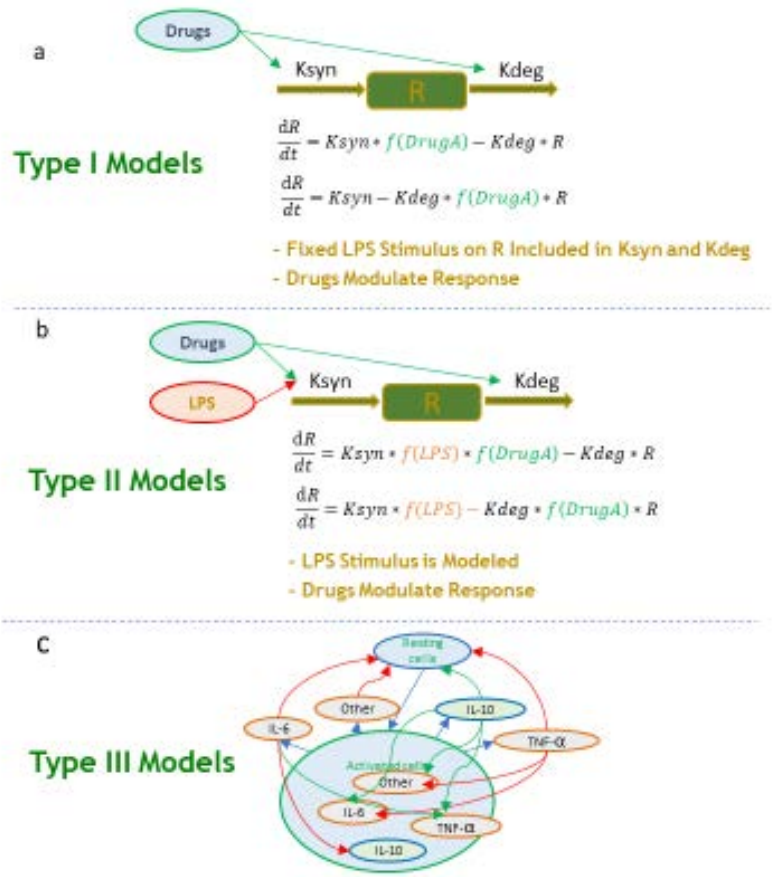

Figure 4. Type of turnover PK-PD models. **a.** Model I: simple turnover model in which the challenger (LPS) is fixed and not included in the model **b**. Model II: the challenger (LPS) is measured and included in the model **c.** Model III: high degree of complexity of PK-PD turnover model in which many factors are included (e.g. bystander cells).

a **Type II MODEL**

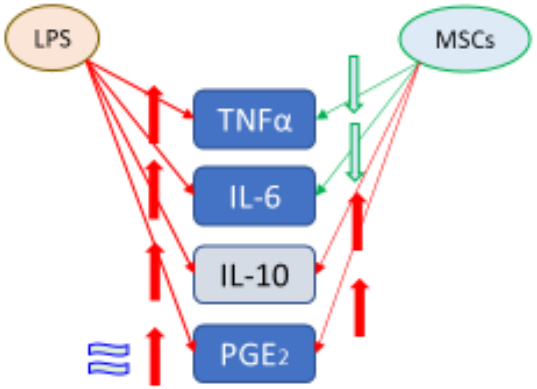

b

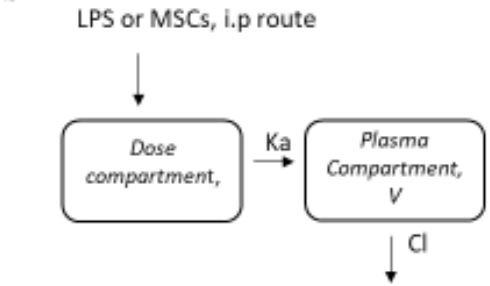

c **Differential Equations**

$$\frac{dA_{LPS}}{dt} = Dose - Ka * A_{LPS}$$

$$\frac{V\, d[C_{LPS}]}{dt} = Ka * A_{LPS} - Cl * C_{LPS}$$

LPS Pharmacokinetic

$$\frac{dA_{MSCs}}{dt} = Dose - Ka * A_{MSCs}$$

$$\frac{V\, d[C_{MSCs}]}{dt} = Ka * A_{MSCs} - Cl * C_{MSCs}$$

MSCs Pharmacokinetic

$$\frac{d[TNF\alpha]}{dt} = Ksyn * \left[1 + \frac{Smax * C^n}{EC_{50_{LPS}}^n + C^n} * \left(1 - \frac{Imax * C^n}{EC_{50_{MSCs}}^n + C^n}\right)\right] - Kdeg * [TNF\alpha]$$

$$\frac{d[IL6]}{dt} = Ksyn * \left[1 + \frac{Smax * C^n}{EC_{50_{LPS}}^n + C^n} * \left(1 - \frac{Imax * C^n}{EC_{50_{MSCs}}^n + C^n}\right)\right] - Kdeg * [IL6]$$

$$\frac{d[IL10]}{dt} = Ksyn * \left[1 + \frac{Smax * C^n}{EC_{50_{LPS}}^n + C^n} * \left(1 + \frac{Smax * C^n}{EC_{50_{MSCs}}^n + C^n}\right)\right] - Kdeg * [IL10]$$

$$\frac{d[PGE2]}{dt} = Ksyn * \left[1 + \left(\frac{Smax * C^n}{EC_{50_{LPS}}^n + C^n}\right) * \left(1 + \frac{Smax * C^n}{EC_{50_{MSCs}}^n + C^n}\right)\right] - Kdeg * [PGE2]$$

Cytokine Effect

Figure 5. Type II model PK-PD for MSCs in sepsis murine model LPS-induced. **a**. Multipotent mesenchymal stromal/stem cells (MSCs) and LPS influence PGE2, IL-6, IL-10 and TNF-α cytokines. Red arrows represent positive stimulus or secretion, green arrows represent negative stimulus or inhibition. **b**. Dose and central (plasma) compartment for MSCs and LPS after i.p administration. The dose compartment is described by the following equations: $\frac{dA_{LPS}}{dt} = Dose - Ka * A_{LPS}$ for LPS, and $\frac{dA_{MSCs}}{dt} = Dose - Ka * A_{MSCs}$ for MSCs; the central compartment rules the following equations: $\frac{V\, d[C_{LPS}]}{dt} = Ka * A_{LPS} - Cl * C_{LPS}$ for LPS, and $\frac{V\, d[C_{MSCs}]}{dt} = Ka * A_{MSCs} - Cl * C_{MSCs}$ for MSCs **c**. The cytokine effect over the time course is described by the differential equations of the PK-PD model II. The type II PK-PD model takes into consideration both the LPS and MSC effect.

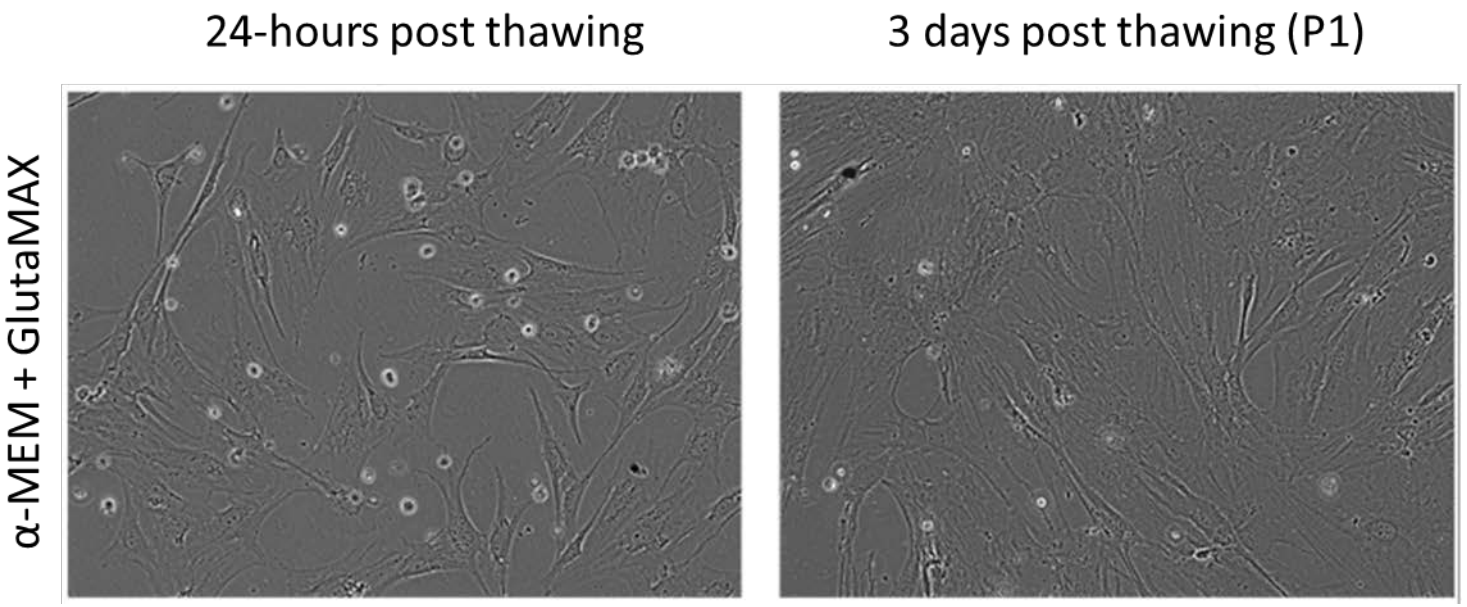

Figure 6. BM-MSCs Morphology. 24 hours and third day post thawing of BM-MSCs plated with α-MEM + GlutaMAx and human PL supplemented. The third day BM-MSCs showed a nice morphology.

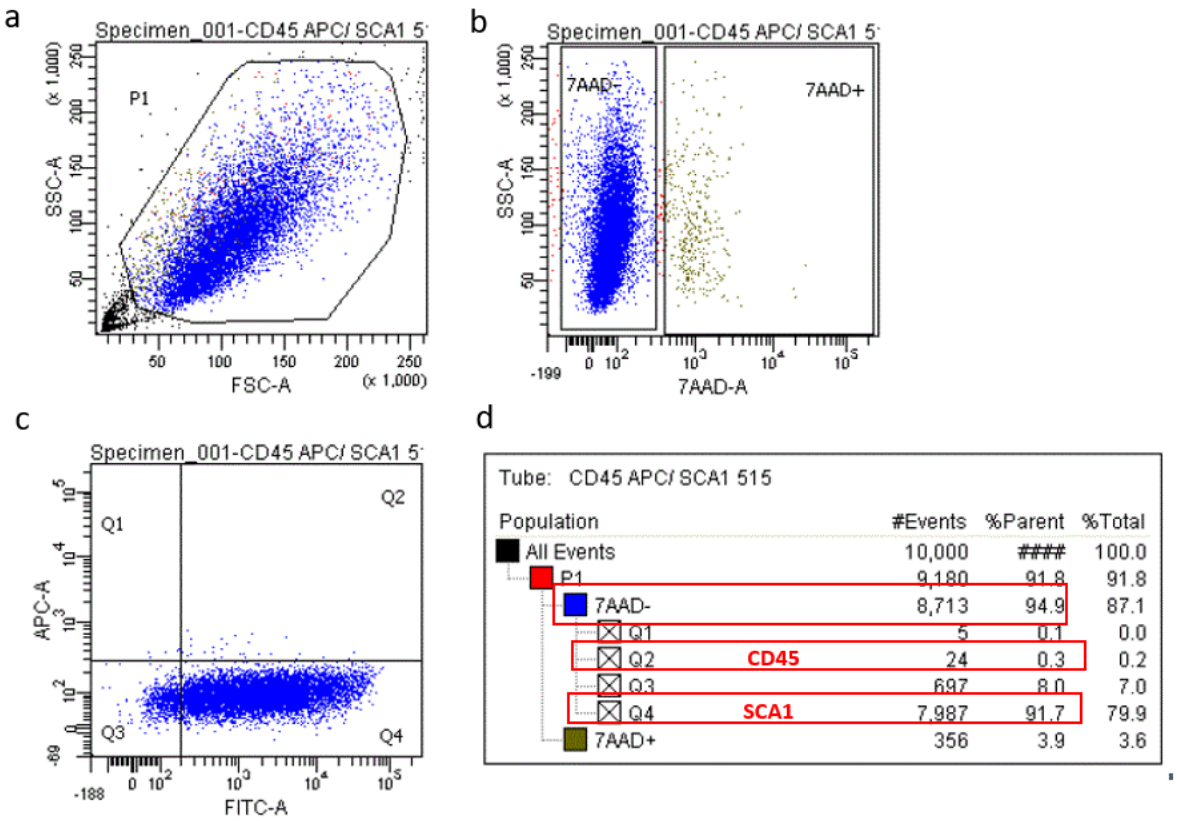

Figure 7. FACS analysis of BM-MSCs. a. Detection of murine MSCs basing on the granularity (SSC-A) and size (FSC-A). **b.** Detection of alive cells, negative for the apoptotic marker surface 7AAD ($7AAD^-$). **c e d**. Detection of CD45 and SCA1 marker surface in order to distinguish between the hematopoietic (CD45+) and mesenchymal stromal ($CD45^-$ SCA1+) lineages.

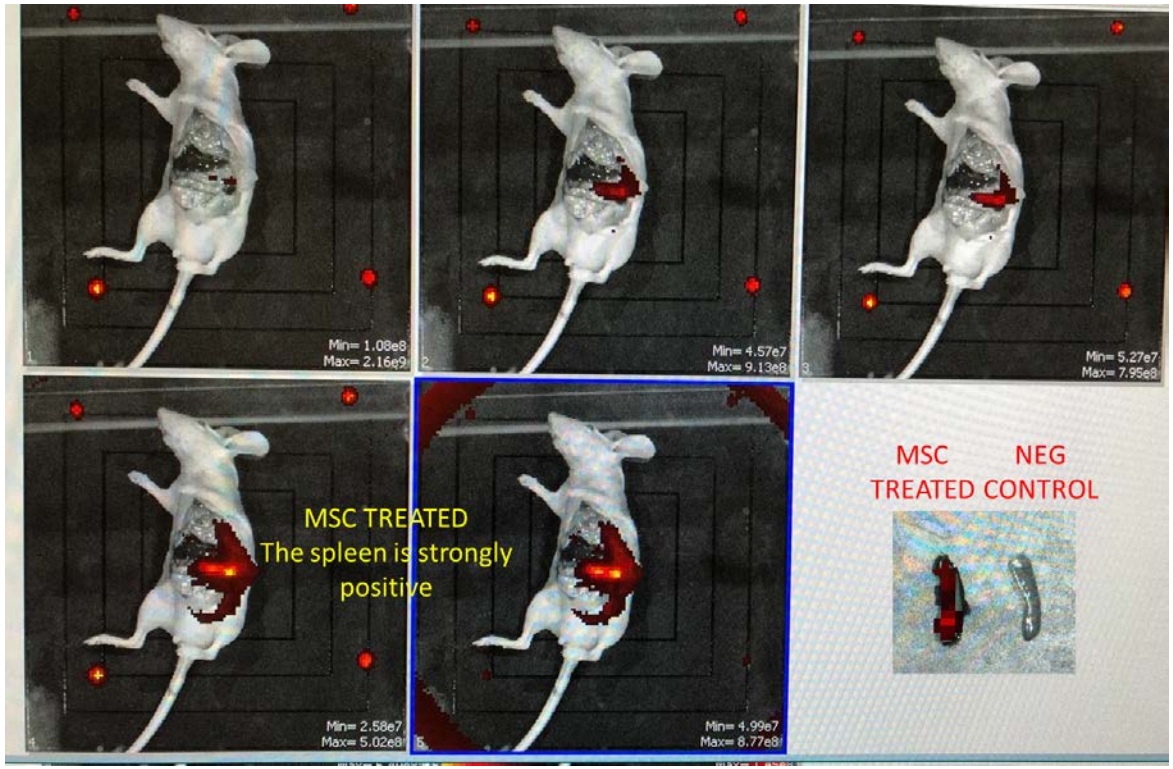

Figure 8. BM-MSCs DiR Labelled. IVIS imaging of mice BM-MSCs DiR labelled treated. After 1 hour, no signal was detected (data not shown); after 24 hours the fluorescence was visibly marked in the abdominal part. In particular, the spleen was strongly fluorescent

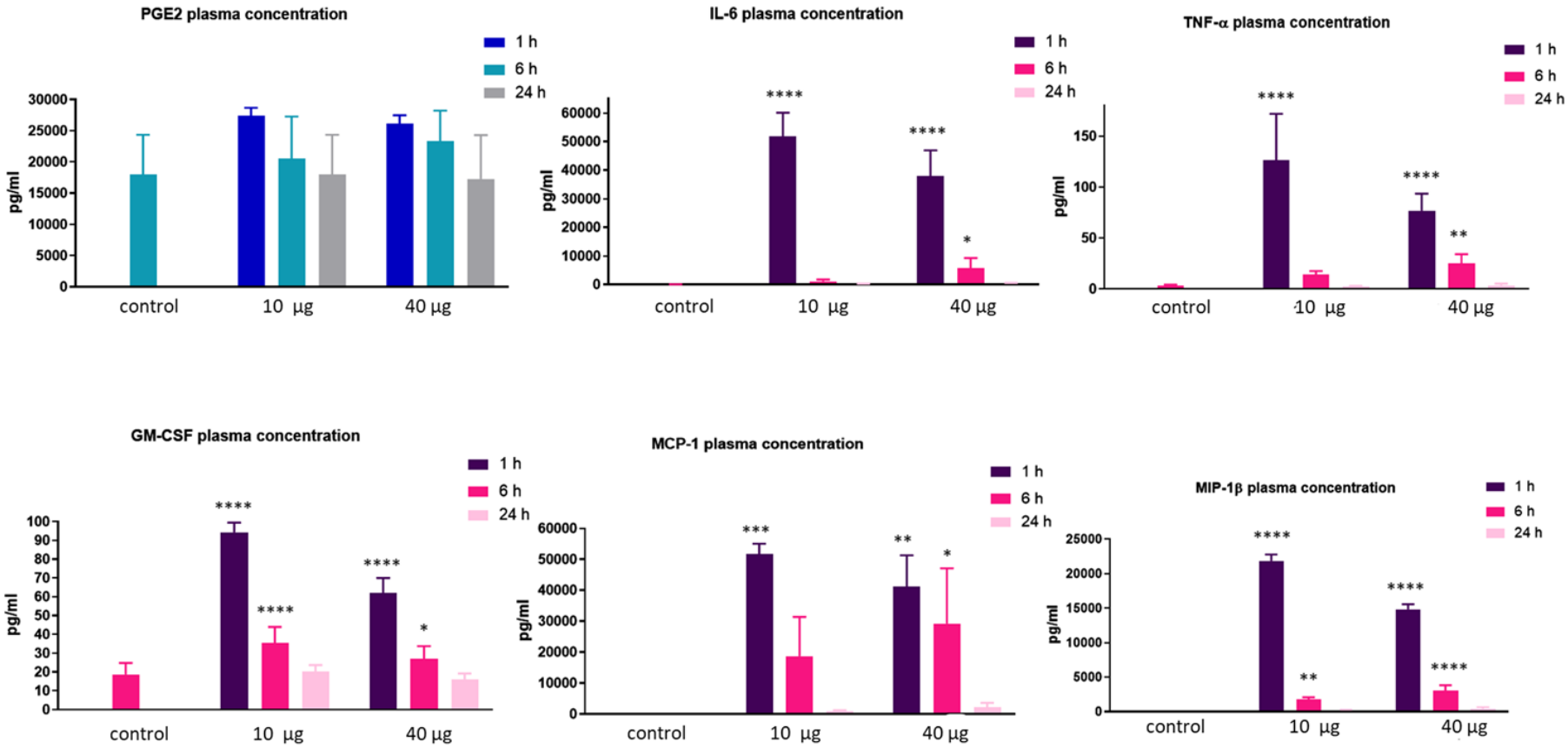
PGE2 plasma concentration
1 h
6 h
24 h
pg/ml
30000
25000
20000
15000
10000
5000
0
control
10 µg
40 µg
IL-6 plasma concentration
1 h
6 h
24 h
pg/ml
60000
50000
40000
30000
20000
10000
0
****
****
*
control
10 µg
40 µg
TNF-α plasma concentration
1 h
6 h
24 h
pg/ml
150
100
50
0
****
****
**
control
10 µg
40 µg
GM-CSF plasma concentration
1 h
6 h
24 h
pg/ml
100
90
80
70
60
50
40
30
20
10
0
****
****
****
*
control
10 µg
40 µg
MCP-1 plasma concentration
1 h
6 h
24 h
pg/ml
60000
50000
40000
30000
20000
10000
0
***
**
*
control
10 µg
40 µg
MIP-1β plasma concentration
1 h
6 h
24 h
pg/ml
25000
20000
15000
10000
5000
0
****
**
****
****
control
10 µg
40 µg

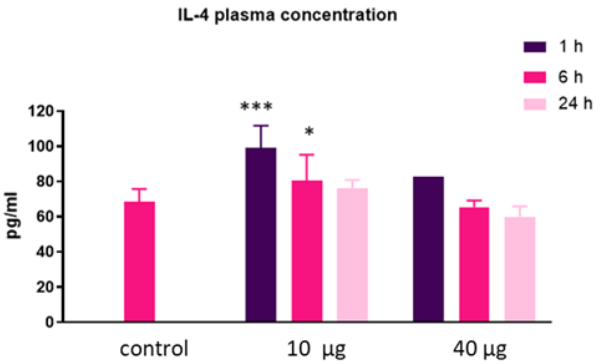
IL-4 plasma concentration
1 h
6 h
24 h
pg/ml
120
100
80
60
40
20
0
***
*
control
10 µg
40 µg

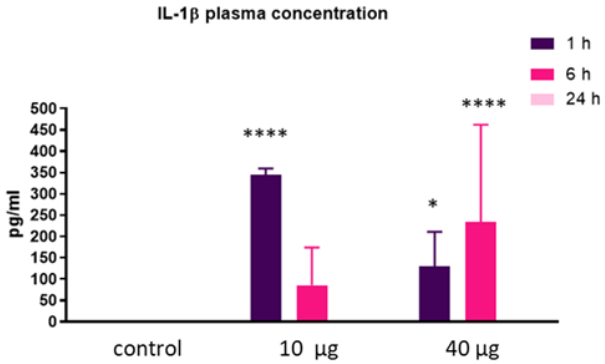
IL-1β plasma concentration
1 h
6 h
24 h
pg/ml
500
450
400
350
300
250
200
150
100
50
0
****
*
****
control
10 µg
40 µg

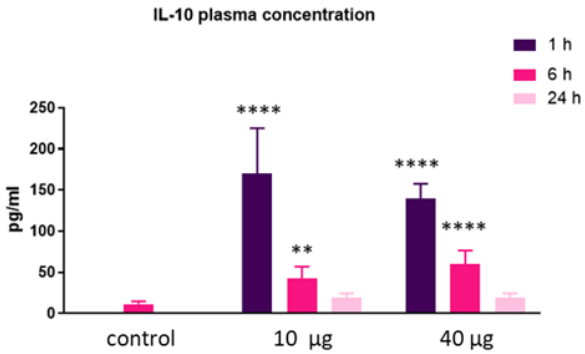
IL-10 plasma concentration
1 h
6 h
24 h
pg/ml
250
200
150
100
50
0
****
**
****
****
control
10 µg
40 µg

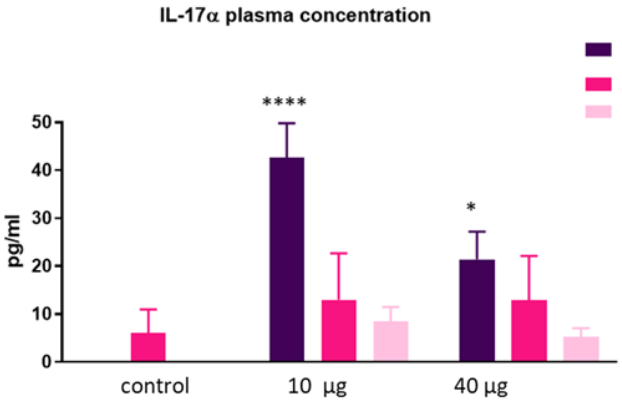
IL-17α plasma concentration
1 h
6 h
24 h
pg/ml
50
40
30
20
10
0
****
*
control
10 µg
40 µg

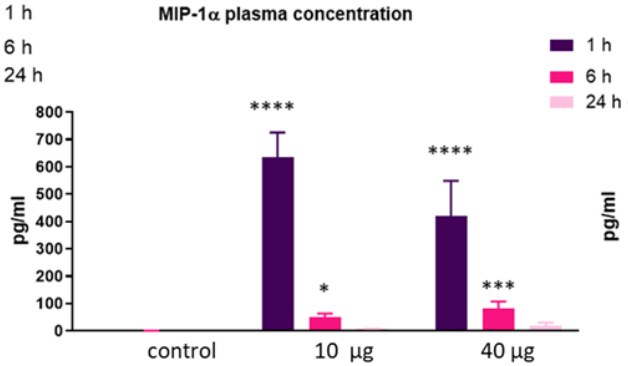
MIP-1α plasma concentration
1 h
6 h
24 h
pg/ml
800
700
600
500
400
300
200
100
0
****
*
****
***
control
10 µg
40 µg

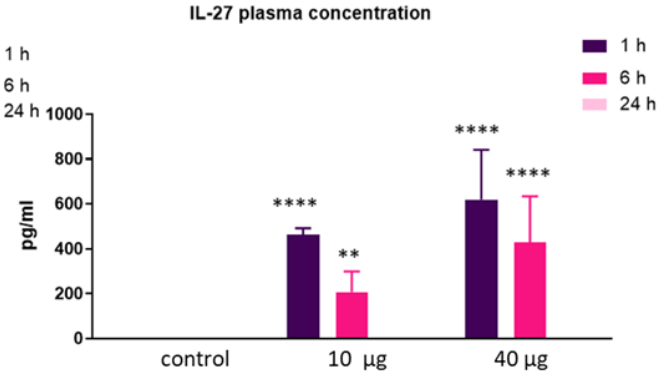
IL-27 plasma concentration
1 h
6 h
24 h
pg/ml
1000
800
600
400
200
0
****
**
****
****
control
10 µg
40 µg

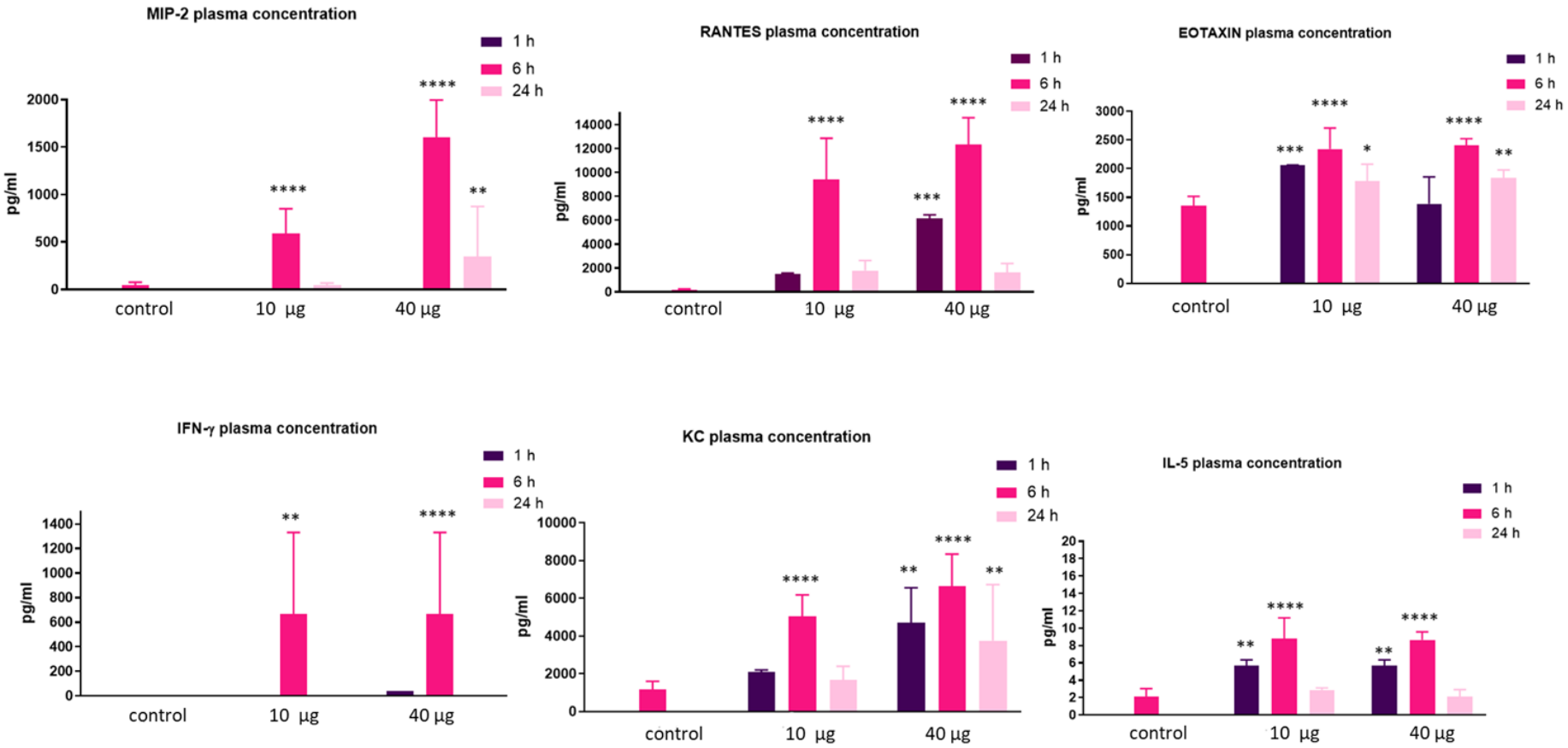
MIP-2 plasma concentration
1 h
6 h
24 h
pg/ml
2000
1500
1000
500
0
****
****
**
control
10 µg
40 µg
RANTES plasma concentration
1 h
6 h
24 h
pg/ml
14000
12000
10000
8000
6000
4000
2000
0
****
****
***
control
10 µg
40 µg
EOTAXIN plasma concentration
1 h
6 h
24 h
pg/ml
3000
2500
2000
1500
1000
500
0
***
****
*
****
**
control
10 µg
40 µg
IFN-γ plasma concentration
1 h
6 h
24 h
pg/ml
1400
1200
1000
800
600
400
200
0
**
****
control
10 µg
40 µg
KC plasma concentration
1 h
6 h
24 h
pg/ml
10000
8000
6000
4000
2000
0
****
**
****
**
control
10 µg
40 µg
IL-5 plasma concentration
1 h
6 h
24 h
pg/ml
20
18
16
14
12
10
8
6
4
2
0
**
****
**
****
control
10 µg
40 µg

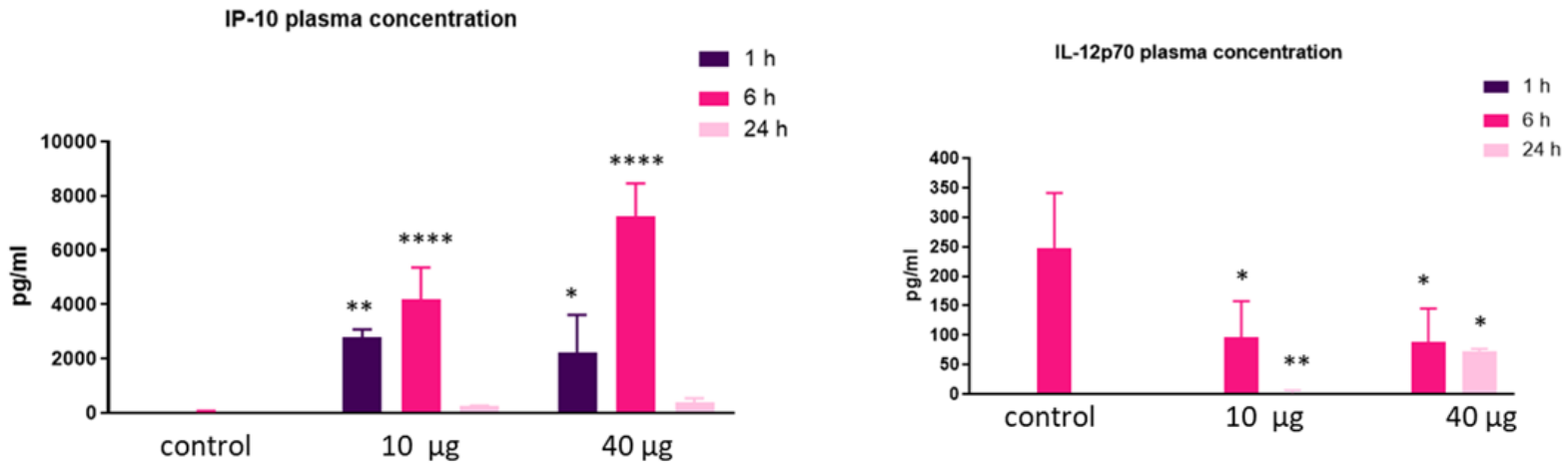

Figure 9. Cytokine quantification in plasma. Histograms of cytokines quantified in plasma 1, 6, 24 hours following a single injection of LPS 10 or 40 µg by i.p in SKH1 mice. Control group cytokine measurement was performed only at 6 hours. Individual bars were plotted as mean ± SD per time point. Data were analysed by two-way ANOVA followed by Tukey's multiple comparisons test, * $p \leq 0.05$, ** $p \leq 0.01$, *** $p \leq 0.001$, **** $p \leq 0.0001$ compared to control

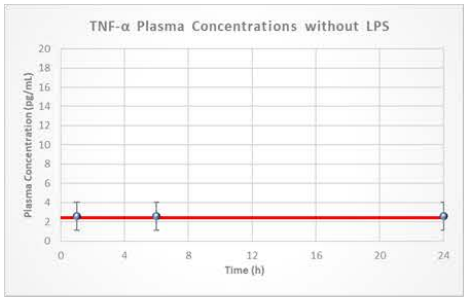

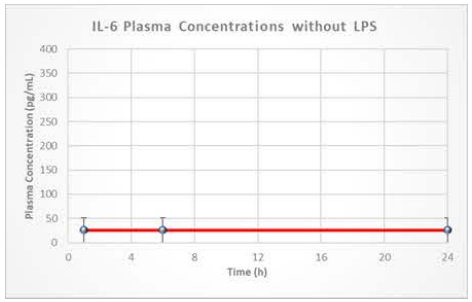

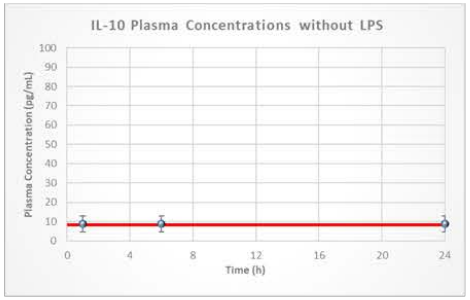

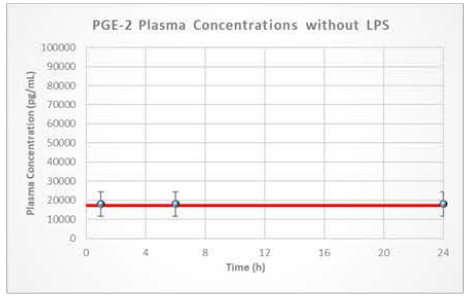

W/O LPS

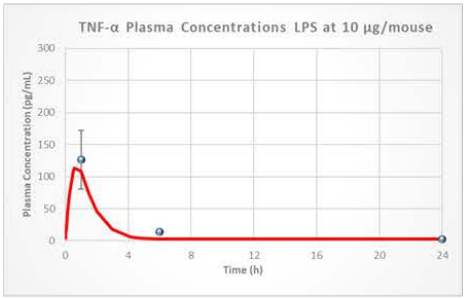

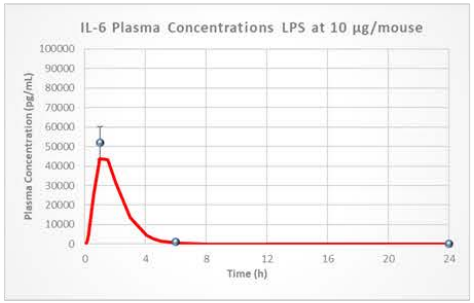

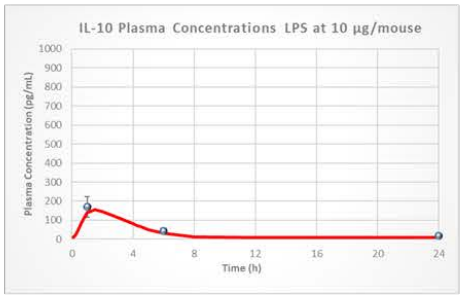

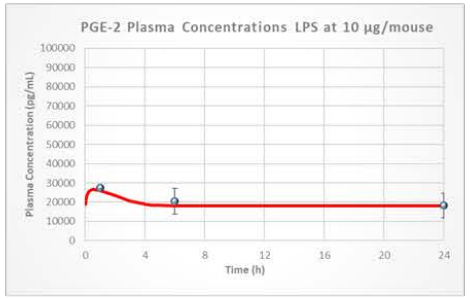

10 µg LPS

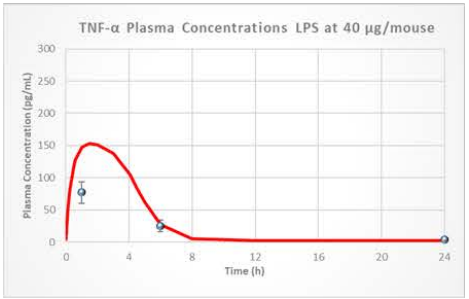

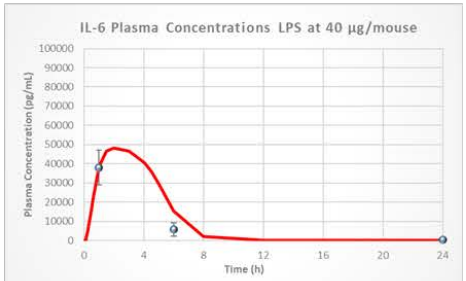

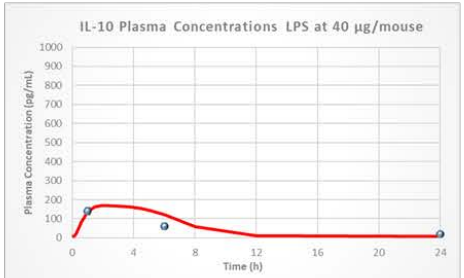

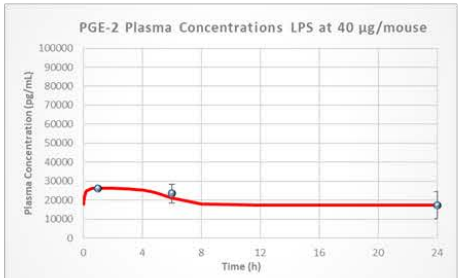

40 µg LPS

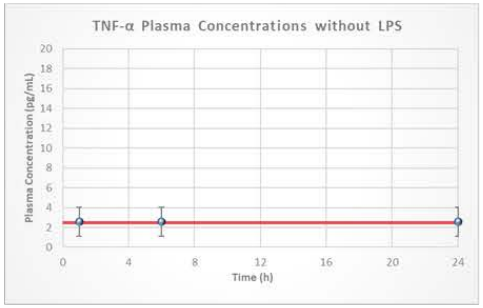

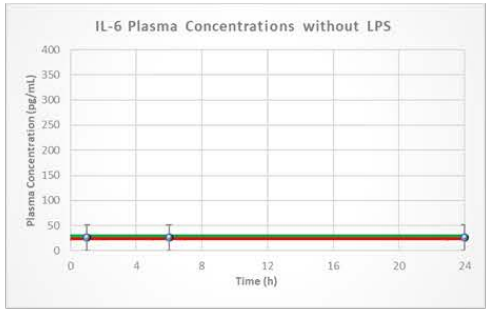

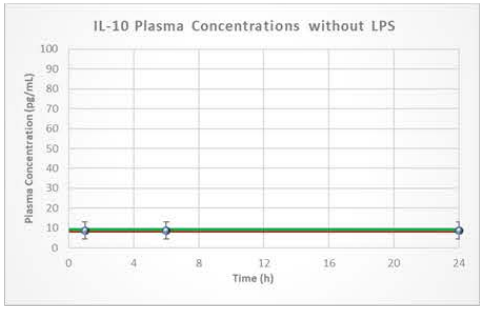

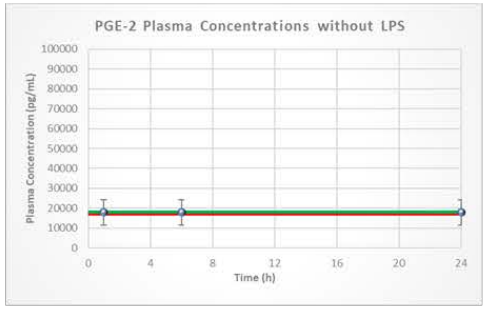

W/O LPS

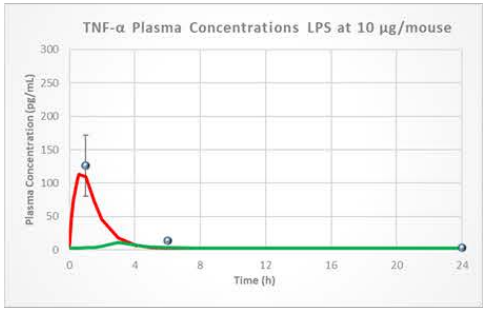

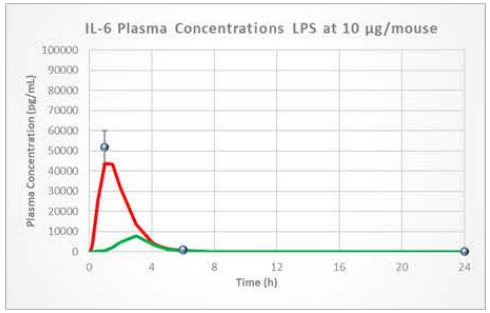

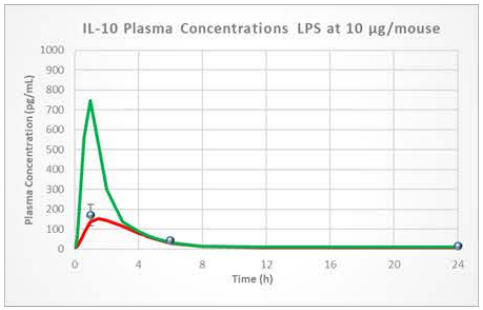

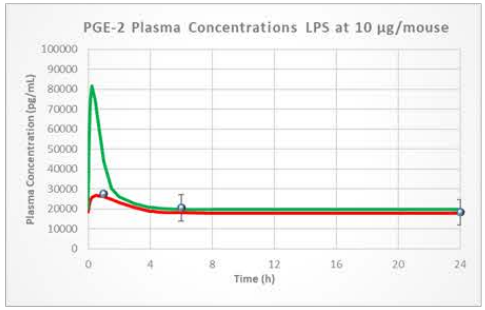

10 µg LPS

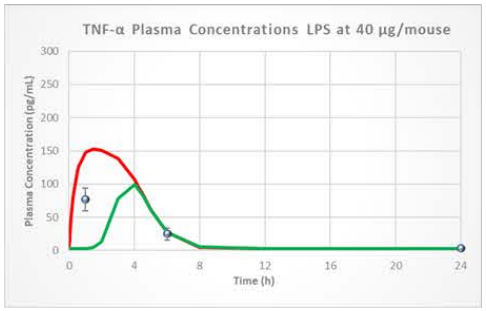

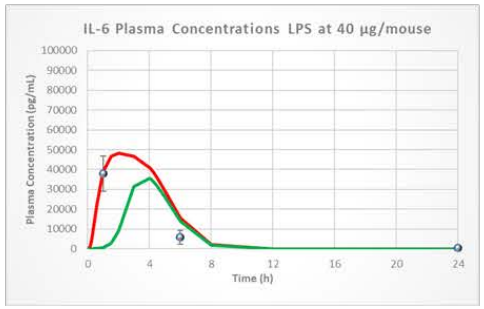

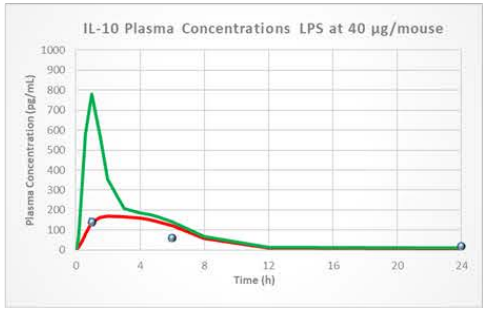

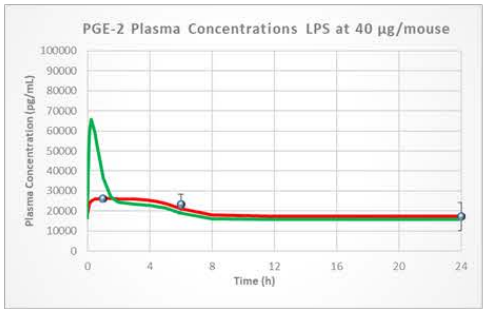

40 µg LPS

Figure 10. Plot of PK-PD Model II. Cytokine kinetic profiles versus time of observed and simulated data in vehicle (without LPS) low (10 μg/mouse) and high dose (40 μg/mouse) LPS groups. Blue dots represent the experimental data; Red lines represent the biomarkers simulated plasma profile of cytokines without MSC effect. Green lines represent the biomarkers simulated plasma profile of cytokines with MSC effect Observed data are mean ± SD; Simulation curve profile is a mean of simulated data got from Model II differential equations.

TABLES

Table 1. Biodistribution Studies of MSCs in Preclinical Settings

Authors	Treatment-related parameters					Lung trapping	Tracking methods		Endpoints
	Model	MSC-source	Labelling	Route	Dose		In vivo read-out	Ex vivo read-out	
A. H. Piersma et al., 1983	Irradiated mouse	Murine BM CFU-F cells	/	i.v.	2-4x10^7/mouse	NO	/	Chromosome-marked donor	CFU-F cells distribution
R. F. Pereira et al.; 1995	Irradiated mouse	Transgenic marrow mice	/	i.v.	1-6x10^5/mouse	YES	/	PCR	Tissue distribution
K. W. Liechty et al., 2000	Fetal sheep early in gestation	Human BM	Fluorescein	i.p. into the fetus	1x10^8-2x10^8/kg	NO	/	*In situ* hybridization Immunohistochemistry PCR	Tissue distribution

Authors	Treatment-related parameters					Lung trapping	Tracking methods		Endpoints
	Model	MSC-source	Labelling	Route	Dose		In vivo read-out	Ex vivo read-out	
J. Gao et al., 2001	Rat	Rat BM	^{111}In-oxine radiolabel	i.a., i.v., and i.p.	1-1.3x10^6/rat	YES	Whole body scanning and real-time monitoring with scintillation camera	/	Organ distribution
C. Niyibizi et al., 2004	Neonatal mouse	Murine BM	eGFP cDNA; ALP activity	i.v.	5x10^4/mouse	YES	Whole body imaging with fluorescence microscopy	Immunofluorescence and Western blot (GFP)	Organ / tissue distribution
S. Schrepfer et al., 2007	Mouse	Murine	Luciferase and green fluorescent dye CSFE	i.v.	0.5x10^6/mouse	YES	BLI	Histopathology: H&E, CSFE staining by microscopy	Organ distribution

Authors	Treatment-related parameters					Lung trapping	Tracking methods		Endpoints
	Model	MSC-source	Labelling	Route	Dose		In vivo read-out	Ex vivo read-out	
L. Zangi et al., 2009	Mouse	Murine BM	Luciferase	i.v., i.p.	$2x10^6$/mouse	YES	BLI	Staining for specific markers and H&E	Tissue distribution
R. H. Lee et al., 2009	Mouse with myocardial infarction	Human BM	N/A	i.v., i.a.	$2x10^6$/mouse	YES	N/A	Real time PCR (Alu seq. and GAPDH), ELISA, siRNA, microarray, histopathology by Masson Trichrome	Tissue distribution, release of therapeutic protein, heart pathology
J-l. Cheng et al., 2010	Traumatic brain injury in rat	Rat BM	SPIO	Intracerebral (stereotaxic)	$0.5x10^6$/rat	N/A	MRI	Prussian blue staining by contrast phase and electronic microscopy	Brain distribution and characterization of MSC

Authors	Treatment-related parameters					Lung trapping	Tracking methods		Endpoints
	Model	MSC-source	Labelling	Route	Dose		In vivo read-out	Ex vivo read-out	
T. H. Kim et al., 2010	Liver cirrhosis in rat	Rat BM	MNP and SPIO	Intrasplenic	$3x10^6$/rat	NO	MRI	H&E and Masson-trichrome sections by electronic microscopy, fluorescent DAPI image analysis by confocal microscope	Organ/tissue distribution and characterization of the MSCs (pre-implant)
S.Y. Nam et al., 2012	Rat model	Rat	Au NTs	i.m.	$1x10^5$ /rat	NO	US/PA	US/PA	Tissue distribution and quantification of MSCs
C. Wu et al., 2014	Rat model of liver injury	Rat BM	Luciferase and RFP (pDNA)	s.m.v.	$2x10^6$/rat	NO	BLI and MRI	Real time PCR and Western blot,	Organ/tissue distribution; characterization of MSC (pre-

Authors	Treatment-related parameters					Lung trapping	Tracking methods		Endpoints
	Model	MSC-source	Labelling	Route	Dose		In vivo read-out	Ex vivo read-out	
			and PAI/SPION					Prussian blue and H&E staining	implant; transaminases levels
M. A. Hossain et al., 2014	Mouse model	Human BM	ATPS-MNP	i.m.	/	NO	MRI	Histopathology : Prussian blue by electron microscope	Organ/tissue distribution
FJ. Wang et al., 2015	Mouse	Human BM	Luciferase and [^{99m}Tc]-HMPAO	i.a. or i.v.	1x10^{6}/mouse	YES higher for i.v. than i.a.	BLI and scintigraphy	Histology, immunohistochemistry (Alu sequence) and qPCR	Organ/tissue distribution
S. M. Kim et al., 2016	Glioma xenograft mouse	Human BM	NIR675 and GFP	i.v.	1x10^{6}/mouse	YES	Near-infrared and visible spectra fluorescence imaging	Histology, immunohistochemistry and qPCR	Organ/brain tissue distribution

ALP, Alkaline phosphatase; Au NTs, gold nanotracers; ATPS, aminopropyltriethoxysilane iron oxide; BLI, bioluminescence imaging; BM, bone marrow; cDNA, complementary DNA; CFU-F, fibroblast colony-forming units; CSFE, 5-(and -6)-carboxyfluorescein diacetate succinimidyl ester; DAPI, 4',6-diamidino-2-phenylindole; eGFP, enhanced green fluorescent protein; ELISA, enzyme-linked immunosorbent assay; GAPDH, glyceraldehyde 3-phosphate dehydrogenase; GFP, green fluorescent protein; H&E hematoxylin and eosin; i.a, intra-artery; i.m, intramuscularly; i.p, intra-peritoneal; i.v, intravenous; MRI, Magnetic resonance imaging; MNP, metal nanoparticle; NIR675, near-infrared 675; NOD, non obese diabetic; PA, photoacoustic; PAI, poly(ethylene glycol)-block-poly(l-aspartic acid)-grafted polyethylenimine; pDNA, plasmids DNA; PCR, polymerase chain reaction; qPCR, quantitative polymerase chain reaction; RFP, red fluorescent protein; siRNA, small interference RNA; s.m.v, superior mesenteric vein; SPIO, superparamagnetic iron oxide; SPION, superparamagnetic iron oxide nanoparticles; ^{99m}Tc-HMPAO; ^{99m}Tc-hexamethyl propylene-amine-oxime; US, ultrasound.

Table 2. Key Findings from Preclinical Studies on MSC Biodistribution

	Findings	**References**
a	MSCs are transplantable cells via the intravenous route	33
b	MSCs are trapped in the lung after systemic administration	34
c	The route of administration and the pulmonary vessel size influence lung trapping	35,36
d	Intrinsic MSC properties and microenvironment cues can affect their biodistribution	37,39
e	Immunity plays a role in MSC biodistribution	40,41,42,43,44,45,46,48
f	Inflammation and cancer influence MSC biodistribution	50,51,52,53,54,55,56,57,58
g	An MSC local delivery is more appropriate for an in situ focal regenerative impact	56,57,58,59,60
h	The reported immunogenicity of MSC allowed pre-clinical investigation in auto-, allo-, and xenogeneic recipients	40,41,42,43,44,45,46,48
i	MSCs can restore tissues due to their intrinsic properties and cross-talk with the target pathological environment	50,51,52,53,54,55,56,57,58
j	Bone marrow is the most selected source for MSCs	33,34,35,37,40,48,50,51,54,56,57,58,60
k	Rodents are appropriate and the most frequently used preclinical models	33,34,35,36,37,48,50,51,54,56,57,58,59,60
l	Intravenous MSC administration is the most applied preclinical route	33,34,35,37,48,50,51,57
m	Combinations of in vivo and ex vivo tracking techniques provide qualitative and quantitative data on MSC distribution over time	37,48,54,56,57,58,59,60

Table 3. Factors Influencing the Planning of a Preclinical Biodistribution Study on MSCs

Pharmacodynamic-related factors
✓ Mechanism of action and therapeutic effects
✓ Target disease localization
✓ Pathophysiology of the disease
✓ Microenvironment
Pharmacokinetic-related factors
✓ MSC related: size, source, donor age and culture passages, culture conditions, and immunogenicity
✓ Non-MSC related: labelling, detection method, animal size, and route of administration

Table 4. Effect of PD-Related Factors on MSC Biodistribution Studies

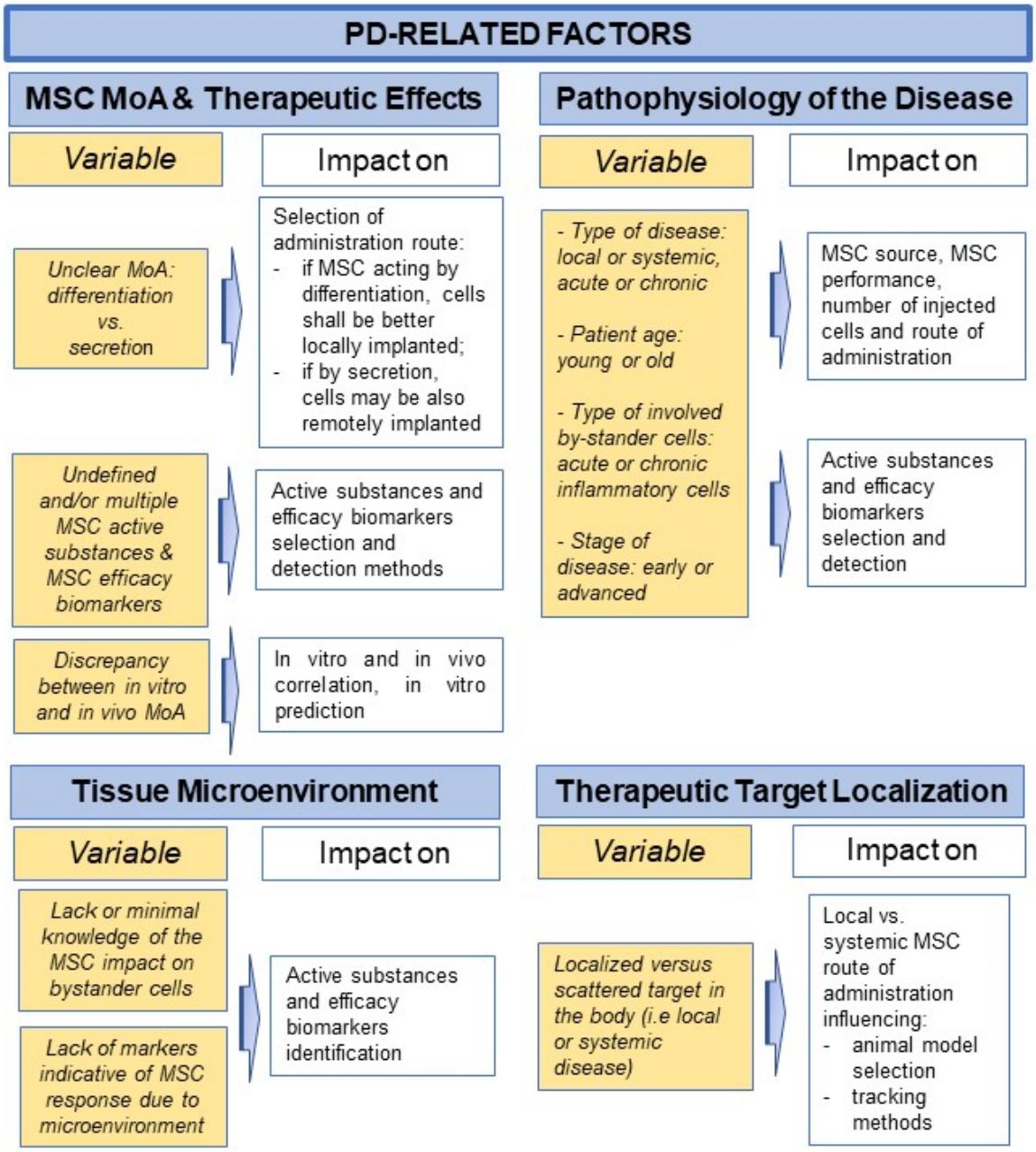

Table 5. Effect of PK-Related Factors on MSC Biodistribution Studies

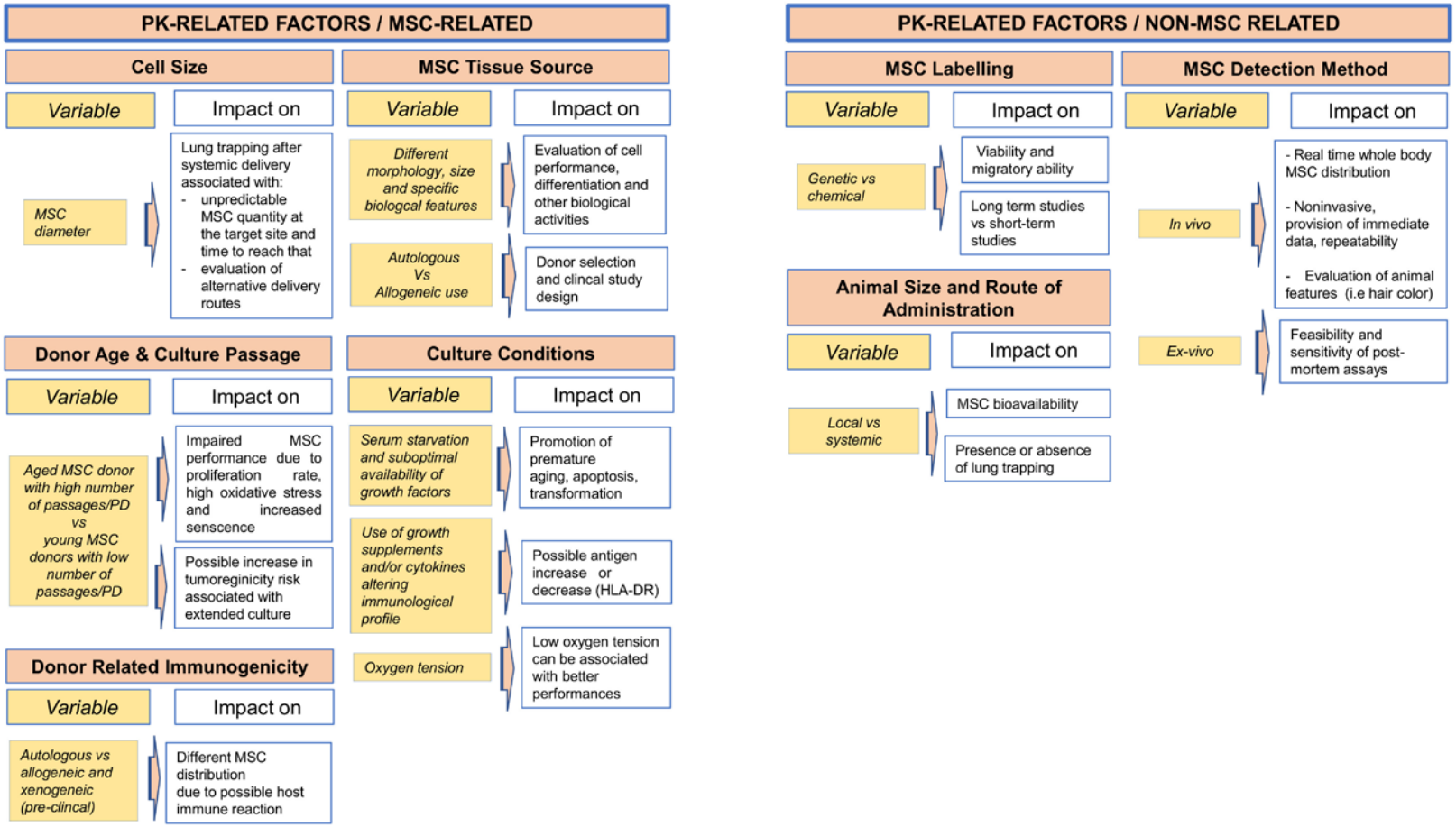

Table 6. MSC Tracking Methods

In vivo imaging	**Explanation and comments**
Fluorescence	Dye on membrane cellular surface; lipophilic carbocyanine dye for whole cell; green fluorescent protein. Easy visualization and no transfer to neighbouring cells, possible cytotoxicity, reduction of signal after mitosis, transfer or phagocytosis of dye to other cells (false positive signal).
Bioluminescence	Luciferase gene report; high follow-up (until 120 days); high tissue specificity, demanding set-up by skilled staff.
Nuclear magnetic resonance	Paramagnetic nanoparticles (Gd); paramagnetic iron oxide-based compound (SPIO, MION, MNP, APTS)- High spatial resolution (25-50 μm), non-invasive, repeatable, clinical setting, high cellular viability, high costs and NMR availability.
Radiolabelling	18F-fluorodeoxyglucose (18F-FDG); indium-111 (111In). Spatial resolution (2 mm) and short-term follow-up (until 48 hours)
Ex vivo assays	
Immunohistochemistry	Selectively imaging antigens (proteins) in cells of a tissue section by exploiting the principle of specific antibodies binding to antigens. High sensitivity and specificity, not high throughput and protocol optimization required
PCR	Amplification of DNA segments. High sensitivity and specificity; quantification method; cheap, fast, and simple testing: high throughput.

GLOSSARY

ADME adsorption distribution metabolism excretion

AMT advanced medicinal therapy

APC antigen-presenting cell

AuNTs Au gold nanotracers

BBB blood-brain barrier

BLI bioluminescence

BM-MSCs bone marrow-mesenchymal stromal cells

BMT bone marrow transplantation

CO2 carbon dioxide

CSFE 5-(and -6)-carboxyfluorescein diacetate succinimidyl ester

EDTA ethylenediaminetetraacetic acid

ELISA enzyme-linked immunosorbent assay

EVs extracellular vesicles

FACS fluorescent activated cell sorting

FBS fetal bovine serum

FDA food and drug administration

GFP green fluorescent protein

GI gastrointestinal

GMCSF granulocyte-macrophage colony-stimulating factor

GVHD graft-versus-host-disease

HLA-DR human leukocyte antigen – DR isotype

hPL human platelet lysate

i.a intra-artery

i.m intra-muscular

i.p intra-peritoneal

i.v intravenous

IFN- γ interferon-γ

IL interleukin

IP-10 interferon γ-induced protein

IVIS in vivo imaging system

KC keratinocyte chemoattractant

LPS lipopolysaccharide

MCP-1 monocyte chemoattractant protein-1

MIP macrophage inflammatory proteins

MoA mechanism of action

MNP metal nanoparticle

MRI magnetic resonance imaging

MSC mesenchymal stromal cell

NIR near infrared fluorescent nanoparticles

NOD non-obese diabetic

PAI poly(ethylene glycol)-block-poly(l-aspartic acid)-grafted polyethylenimine

PCR polymerase chain reaction

PD pharmacodynamic

PET positron emission tomography

PGE2 prostaglandine-2

pDNA plasmids DNA

PBPK physiologically based pharmacokinetic modelling

PBS Phosphate buffer solution

PK pharmacokinetic

S serial

SPECT single photon emission computed tomography

SCID severe combined immunodeficiency

SD standard deviation

SE standard error

SEM standard error of the mean

SPIO superparamagnetic iron oxide

SPION superparamagnetic iron oxide nanoparticles

T terminal

TNF-α tumour necrosis factor α

TSG-6 TNF-stimulated gene 6 protein

SPIO superparamagnetic iron oxide

US/PA ultrasound and photoacoustic imaging

α-MEM α-minimum essential medium eagle

7-AAD 7-aminoactinomycin D

3-TMRI 3-T magnetic resonance imaging

ACKNOWLEDGEMENTS

I would like to thank my tutor Massimo Dominici for giving me the opportunity to get to know the fascinating world of MSCs.

Thanks to Paola, Benedetta and Nicola for giving me help and essential suggestions.

Thanks to my friend Alba, whose work was essential for the success of this thesis.

Thanks to Massimiliano Dall'Ora, Giulia Grisendi, Ilenia Mastrolia, Filippo Rossignoli for the great job!

Thanks to my family, without their teachings I would have never achieved this goal.

Last but not least, I would like to thank myself for never giving up and always believing that I could reach this goal.

REFERENCES

[1] Parekkadan, B. and Milwid, JM. (2010). Mesenchymal stem cells as therapeutics. *Annu Rev Biomed Eng.* USA 12, 87–117.

[2] Squillaro, T., Peluso, G., Galderisi, U. Clinical trials with mesenchymal stem cells: an update. *Cell Transplantation.* 25, 829-848 (2016).

[3] Hass, R., Kasper, C., Böhm S., Jacobs, R., (2011). Different populations and sources of human mesenchymal stem cells (MSC): a comparison of adult and neonatal tissue-derived MSC. *Cell Commun Signal.* 14, 9-12 (2011).

[4] Marquez-Curtis, LA., Janowska-Wieczorek, A., McGann, EL., Elliotta, J. AW. Mesenchymal stromal cells derived from various tissues: biological, clinical and cryopreservation aspects. *Cryobiology.* 71(2), 181-197 (2015).

[5] Matsumoto, T. and Mugishima, H. Non-Hematopoietic stem cells in umbilical cord blood. *Int J Stem Cells.* 2(2), 83-89 (2009).

[6] Rustad, KC. and Gurtner, GC. Mesenchymal stem cells home to sites of injury and inflammation. *Adv Wound Care.* 1(4), 147-152 (2012).

[7] De Becker, A. and Van Riet, I. Homing and migration of mesenchymal stromal cells: how to improve the efficacy of cell therapy? *World J Stem Cells.* 8(3), 73-87 (2016).

[8] Sheng, G. The developmental basis of mesenchymal stem/stromal cells (MSCs). *BMC Dev Biol.* 15, 44 (2015).

[9] Vellasamy, S., Tong, CK., Azhar, NA., Kodiappan, R., Chan, SC., Veerakumarasivam, A. et al. Human mesenchymal stromal cells modulate T-cell immune response via transcriptomic regulation. *Cytotherapy.* 18(10), 1270-83 (2016).

[10] Fibbe, WE., Nauta, AJ., Roelofs, H. Modulation of immune responses by mesenchymal stem cells. *Ann. N.Y. Acad. Sci.* 1106, 272-278 (2007).

[11] Ullah, I., Subbarao, RB., Rho, GJ. (2015). Human mesenchymal stem cells - current trends and future prospective. *Biosci Rep.* 8, 35(2) (2015). Republic of Korea doi:10.1042/BSR20150025.

[12] Kyurkchiev, D., Bochev, I., Ivanova-Todorova, E., Mourdjeva, M., Oreshkova, T., Belemezova, K. et al. Secretion of immunoregulatory cytokines by mesenchymal stem cells. *World J Stem Cells.* 6(5), 552–570 (2014).

[13] Maiti, S. K., Ninu, AR., Sangeetha, P., Mathew, DD., Tamilmahan, P., Kritaniya, D. et al. Isolation, Proliferation and morphological characteristics of bone-marrow derived mesenchymal stem cells (BM-MSC) from different animal species. *Trends Biomater. Artif. Organs.* 27(1), 29-35 (2013).

[14] Le Blanc, K., Rasmusson, I., Sundberg, B., Gotherstrom, C., Hassan, M., Uzunel, M. et al. (2004). Treatment of severe acute graft-versus-host disease with third-party haploidentical mesenchymal stem cells. *Lancet.* 1, 363(9419), 1439-41 (2004).

[15] Gu, L-H., Zhang, TT., Li, Y., Yan, HJ., Qi, H., Li, FR. Immunogenicity of allogeneic mesenchymal stem cells transplanted via different routes in diabetic rats. *Cell Mol Immunol.* 12(4), 444-445 (2015).

[16] De Girolamo, L., Lucarelli, E., Alessandri, G, Avanzini, MA., Bernardo, ME., Biagi, E., et al. (2013). Mesenchymal stem/stromal cells: a new "cells as drugs" paradigm. Efficacy and critical aspects in cell therapy. *Curr Pharm Des.* Italy 19(13), 2459-73 (2013).

[17] Prockop, D. J. and Oh, J. Y. Mesenchymal stem/stromal cells (MSCs): role as guardians of inflammation. *Mol Ther*. 20(1), 14-20 (2011).

[18] Hocking, A. M. and Gibran, N. S. Mesenchymal stem cells: paracrine signaling and differentiation during cutaneous wound repair. *Exp Cell Res*. 316(14), 2213–2219 (2010).

[19] Parekkadan, B., van Poll, D., Suganuma, K., Carter, EA., Berthiaume, F., Tilles, AW. et al. Mesenchymal stem cell-derived molecules reverse fulminant hepatic failure. *PLoS One.* 2, e941 (2007).

[20] Van Poll, D., Parekkadan, B., Cho, CH., Berthiaume, F., Nahmias, Y., Tilles, AW. et al. Mesenchymal stem cell-derived molecules directly modulate hepatocellular death and regeneration in vitro and in vivo. Hepatology. 47, 1634–43 (2008).

[21] Phinney, DG., Prockop, DJ. Coincise review: mesenchymal stem/multipotent stromal cells: the state of transdifferentiation and modes of tissue repair-current views. *Stem Cells*. 25(11), 2896-902 (2007).

[22] Prockop, DJ. Inflammation, fibrosis, and modulation of the process by mesenchymal stem/stromal cells. *Matrix Biol.* 51, 7-13 (2016).

[23] Lee, R. Yu, JM., Foskett, AM., Peltier, G., Reneau, JC., Bazhanov, N. et al. TSG-6 as a biomarker to predict efficacy of human mesenchymal stem/progenitor cells (hMSCs) in modulating sterile inflammation in vivo. *Proc Natl Acad Sci.* USA 111(47), 16766-71 (2014).

[24] Kusuma, G. D., Carthew, J., Lim, R., Frith, J. E. Effect of the microenvironment on mesenchymal stem cell paracrine signaling: opportunities to engineer the therapeutic effect. *Stem Cells Dev.* 26(9), 617-631 (2017).

[25] Leuning, DG., Beijer, NRM., du Fossé, NA., Vermeulen, S., Lievers, E., van Kooten. C. et al. The cytokine secretion profile of mesenchymal stromal cells is determined by surface structure of the microenvironment. *Sci Rep.*8(1), 7716 (2018).

[26] Elman, JS., Murray, RM., Wang, F., Shen, K., Gao, S., Conway, KE. et al. Pharmacokinetics of natural and engineered secreted factors delivered by mesenchymal stromal cells. *PLoS One.* 9(2), e89882 (2014).

[27] Chinnadurai, R. Rajan, D., Qayed, M., Arafat, D., Garcia, M., Liu, Y. et al. Potency analysis of mesenchymal stromal cells using a combinatorial assay matrix approach. *Cell Rep.* 22(9), 2504-2517 (2018).

[28] Oliver-Vila, I., Ramírez-Moncayo, C., Grau-Vorster, M., Marín-Gallén, S., Caminal, M., Vives, J. Optimisation of a potency assay for the assessment of immunomodulative potential of clinical grade multipotent mesenchymal stromal cells. *Cytotechnology.* 70(1), 31-44 (2018).

[29] De Wolf, C. van de Bovenkamp, M. Hoefnagel, M. Regulatory perspective on in vitro potency assays for human mesenchymal stromal cells used in immunotherapy. *Cytotherapy.* 19(7), 784-797 (2017).

[30] Németh, K. Leelahavanichkul, A., Yuen, PS., Mayer, B., Parmelee, A., Doi, K. et al. Bone marrow stromal cells attenuate sepsis via prostaglandin E2-dependent reprogramming of host macrophages to increase the interleukin-10 production. *Nat Med.* 15(1), 42-9 (2009).

[31] D'souza, N., Rossignoli, F., Golinelli, G., Grisendi, G., Spano, C., Candini, O. et al. Mesenchymal stem/stromal cells as a delivery platform in cell and gene therapies. *BMC Med.* 13, 186 (2015).

[32] Valenti, M. T., Mori, A., Malerba, G., Dalle Carbonare, L. Mesenchymal stem cells: a new diagnostic tool? *World J Ste Cell.* 7(5), 789-792 (2015).

[33] Piersma, A., H., Ploemacher, R., E., Brockbank, K., G., (1983). Transplantation of bone marrow fibroblastoid stromal cells in mice via the intravenous route. *Br J Haematol.* Netherlands 54(2), 285-290 (1983).

[34] Pereira, RF., Halford, KW., O'Hara, MD., Leeper, DB., Sokolov, BP., Pollard, MD. et al. Cultured adherent cells from marrow can serve as long-lasting precursor cells for bone, cartilage, and lung in irradiated mice. *Proc Natl Acad Sci* U S A. (92)11, 4857-61 (1995).

[35] Gao, J., Dennis, JE., Muzic, RF., Lundberg, M., Caplan, AI. (2001). The dynamic in vivo distribution of bone marrow-derived mesenchymal stem cells after infusion. *Cells Tissue Organs.* USA 169(1),12-20 (2001).

[36] Schrepfer, S., Deuse, T., Reichenspurner, H., Fischbein, MP., Robbins, RC., Pelletier, MP. et al. Stem cell transplantation: the lung barrier. *Transplantation Proc.* 39(2), 573–6 (2007).

[37] Niyibizi, C., Wang, S., Mi Z., Robbins PD. The fate of mesenchymal stem cells transplanted into immunocompetent neonatal mice: implications for skeletal gene therapy via stem cells *Mol. Ther.* 96, 955-963 (2004).

[38] Ge, J., Guo, L., Wang, S., Zhang, Y., Cai, T., Zhao, RC., et al. The size of mesenchymal stem cells is a significant cause of vascular obstructions and stroke. *Stem Cell Reviews and Reports*. 10(2), 295-303.

[39] Somoza, RA., Welter, JF., Correa, D., Caplan, AI. Chondrogenic differentiation of mesenchymal stem cells: challenges and unfulfilled expectations. *Tissue Eng Part B Rev.* 20(6), 596–608 (2014).

[40] Liechty, KW., MacKenzie, TC., Shaaban, AF., Radu, A., Moseley, AM., Deans, R., et al. Human mesenchymal stem cells engraft and demonstrate site-specific differentiation after in utero transplantation in sheep. *Nat Med.* 6, 1282–86 (2000).

[41] Kovach, TK., Dighe, AS., Lobo, PI., Cu, Q. Interactions between MSCs and immune cells: implications for bone healing. *J Immunol Res*. 2015, 752510 (2015).

[42] D'souza, N., Burns, JS., Grisendi, G., Candini, O., Veronesi, E., Piccinno, S. et al. MSC and tumors: homing, differentiation, and secretion influence therapeutic potential. *Adv Biochem Eng Biotechnol.* 130, 209-66 (2013).

[43] Aggarwal, S., Pittenger, MF. Human mesenchymal stem cells modulate allogeneic immune cell responses. *Blood.* 105(4), 1815-22 (2005).

[44] Ryan, JM., Barry, FP., Murphy, JM., Mahon, BP. Mesenchymal stem cells avoid allogeneic rejection. *J Inflamm (Lond).* (26), 2-8 (2005).

[45] Edelshtein, Y., Ophir, E., Bachar-Lustig, E. Ex-vivo acquisition of central memory phenotype is critical for tolerance induction by donor anti-3rd party CD8 T cells in allogeneic bone marrow transplantation. Blood (ASH Annual Meeting Abstracts). 112, 2323 (2008).

[46] Krampera, M., Cosmi, L., Angeli, R., Pasini, A., Liotta, F., Andreini, A. et al. Role for interferon-gamma in the immunomodulatory activity of human bone marrow mesenchymal stem cells. *Stem Cells.* 24(2), 386-98 (2006).

[47] Grau-Voster, M., Rodriguez, L., Torrents-Zapata, S., Vivas, D., Codinach, M., Blanco, M. et al. Levels of IL-17F and IL-33 correlate with HLA-DR activation in clinical-grade human bone marrow-derived multipotent mesenchymal stromal cell expansion cultures. Cytotherapy. (21), 32-40 (2019).

[48] Zangi, L., Margalit, R., Reich-Zeliger, S., Bachar-Lustig, E., Beilhack, A., Negrin, R. et al. Direct imaging of immune rejection and memory induction by allogeneic mesenchymal stromal cells. *Stem Cells.* (27), 2865-2874 (2009).

[49] Galleu, A., Riffo-Vasquez, Y., Trento, C., Lomas, C., Dolcetti, L., Cheung, TS. et al. Apoptosis in mesenchymal stromal cells induces in vivo recipient-mediated immunomodulation. *Sci Transl Med.* 9(416), (2017).

[50] Wang, FJ., Eid, S., Dennis, JE., Cooke, KR., Auletta, JJ., Lee, Z. Route of delivery influences biodistribution of human bone marrow-derived mesenchymal stromal cells following experimental bone marrow transplantation. *J Stem Cells Regen Med.* 11(2), 34-43 (2015).

[51] Lee, R. H., Pulin, AA., Seo, MJ., Kota, DJ., Ylostalo, J., Larson, BL. et al. Intravenous hMSCs improve myocardial infarction in mice because cells embolized in lung are activated to secrete the anti-inflammatory protein TSG-6. *Cell Stem Cell.* 5(1), 54-63 (2009).

[52] Vaegler, M., Maerz, JK., Amend, B., da Silva, LA., Mannheim, JG., Fuchs, K. et al. Labelling and tracking of human mesenchymal stromal cells in preclinical studies and large animal models degenerative diseases. *Curr Stem Cell Res Therapy*. 9(5), 444-450 (2014).

[53] Shah, K. Mesenchymal stem cells in cancer therapy. *Elsevier* (2014).

[54] Kim, SM., Jeong, CH., Woo, JS., Ryu, CH., Lee, JH., Jeun, SS. In vivo near-infrared imaging for tracking of systemically delivered mesenchymal stem cells: tropism for brain tumors and biodistribution. *Int J Nanomedicine*. 11, 13-23 (2016).

[55] Liu, L., Eckert, MA., Riazifar, H., Kang, DK., Agalliu, D., Zhao, W. From blood to the brain: can systemically transplanted mesenchymal stem cells cross the blood-brain barrier? *Stem Cells Int.* 2013, 435093 (2013).

[56] Cheng, JL., Yang, YJ., Li, HL., Wang, J., Wang, MH., Zhang, Y. In vivo tracing of superparamagnetic iron oxide-labeled bone marrow mesenchymal stem cells transplanted for traumatic brain injury by susceptibility weighted imaging in a rat model. *Chin J Traumatol.* China 13(3), 173-177 (2010).

[57] Kim, TH., Kim. JK., Shim, W., Kim, SY., Park, TJ., Jung, JY. Tracking of transplanted mesenchymal stem cells labeled with fluorescent magnetic nanoparticle in liver cirrhosis rat model with 3-T MRI. *Magn Reson Imaging.* 28(7), 1004-13 (2010).

[58] Wu, C., Li, J., Pang. P., Liu, J., Zhu, K., Li, D. et al. Polymeric vector-mediated gene transfection of MSCs for dual bioluminescent and MRI tracking in vivo. *Biomaterials*. China 35(28), 8249-8260 (2014).

[59] Nam, SY., Ricles, LM., Suggs, LJ., Emelianov SY. In vivo ultrasound and photoacoustic monitoring of mesenchymal stem cells labeled with gold nanotracers. *PloS*Plos *one.* USA 7(5), e37267 (2012).

[60] Hossain, MA., Frampton, AE., Bagul A. Challenges facing in vivo tracking of mesenchymal stem cells used for tissue regeneration. *Expert Rev. Med. Devices*. UK 11(1),9–13 (2014).

[61] Mushahary, D., Spittler A., Kasper C., Weber V., Charwat V. Isolation, cultivation, and characterization of human mesenchymal stem cells. *Cytometry A*. 93(1), 19-31 (2018).

[62] Reyes, B., Coca, MI., Codinach, M., López-Lucas, MD., Del Mazo-Barbara, A., Caminal, M. et al. Assessment of biodistribution using mesenchymal stromal cells: algorithm for study design and challenges in detection methodologies. *Cytotherapy.* 19, 1060-1069 (2017).

[63] Liang, X., Ding, Y., Zhang, Y., Tse, H-F., Lian, Q. Paracrine mechanisms of mesenchymal stem cell-based therapy: current status and perspectives. *Cell Transplantation.* 23, 1045–1059 (2014).

[64] Rai, B. Lin, JL., Lim, ZX., Guldberg, RE., Hutmacher, DW., Cool, SM. Differences between in vitro viability and differentiation and in vivo bone-forming efficacy of human mesenchymal stem cells cultured on PCL–TCP scaffolds. *Biomaterials.* 31(31), 7960-7970 (2010).

[65] Si Mui Sim, D. Pharmacological basis of acute care. Springer. Chan, Y. K., Ng, K. P., Sim, D. S. M. 9-15 (2015).

[66] Kean, TJ., Lin, P., Caplan, AL., Dennis, JE. MSCs: delivery routes and engraftment, cell-targeting strategies, and immune modulation. *Stem cells Int.* 2013, 732742 (2013).

[67] Meijers, WC., van der Velde, AR., Muller Kobold, AC., Dijck-Brouwer, J., Wu, AH., Jaffe, A., et al. Variability of biomarkers in patients with chronic heart failure and healthy controls. *European Journal of Heart Failure.* 19, 357–365 (2017).

[68] Caplan, AI. What's in a Name? *Tissue Eng.* Part A 16(8).

[69] Caplan AI. and Correa D. The MSC: An Injury Drugstore. *Cell Stem Cells.* 9(1), 11-15 2011.

[70] Oja, Komulainen, SP., Penttilä, A., Nystedt, J., Korhonen, M. Automated image analysis detects aging in clinical-grade mesenchymal stromal cell cultures. *Stem Cell Research & Therapy* 9(6) (2018).

[71] Niemela, S., Miettinen, S., Sarjanen, JR., Ashammakhi, N. Adipose tissue and adipocyte differentiation: molecular and cellular aspects and tissue engineering applications. Topics in tissue engineering. Vol.4 N Ashammakhi, R Reis, & F Chiellini (2008).

[72] Chen, X., Zhang, F., He, X., Xu, Y., Yang, Z., Chen, L. et al. Chondrogenic differentiation of umbilical cord-derived mesenchymal stem cells in type I collagen-hydrogel for cartilage engineering. *Injury*. 44(4), 540-549 (2013).

[73] Zajdel, A., Kalucka, M., Kokoszka-Mikolaj, E., Wilczok, A. Osteogenic differentiation of human mesenchymal stem cells from adipose tissue and Wharton' s jelly of the umbilical cord. *ACTA ABP Biochimica Polonica*. 64(2), 365-369 (2017).

[74] Viswanathan, S., Keating, A., Deans, R., Hematti, P., Prockop, D., Stroncek, DF. et al. Soliciting strategies for developing cell-based reference materials to advance mesenchymal stromal cell research and clinical translation. *Stem Cells Dev.* 23(11), 1157–1167 (2014).

[75] Wang, H., Jin, P., Sabatino, M., Ren, J., Civini, S., Bogin, V. et al. Comparison of endometrial regenerative cells and bone marrow stromal cells. *J Transl Med.* 10, 207 (2012).

[76] Stolzing, A., Jones, E., McGonagle, D., Scutt, A. Age-related changes in human bone marrow-derived mesenchymal stem cells: consequences for cell therapies. *Mech Ageing Dev.* 129(3), 163-73 (2008).

[77] Gao, F., Chiu, SM., Motan, DA., Zhang, Z., Chen, L., Ji. HL. et al. Mesenchymal stem cells and immunomodulation: current status and future prospects. *Cell Death Dis*. 7, e2062 (2016).

[78] Rubio, D., Garcia, S., Paz, MF., De la Cueva, T., Lopez-Fernandez, LA., Lloyd, AC. et al. Molecular characterization of spontaneous mesenchymal stem cell transformation. *PLoS One*PLoS One. 3(1), e1398 (2008).

[79] Xiao, W., Mohseny, AB., Hogendoorn, PCW., Cleton-Jansen, A-M. Mesenchymal stem cell transformation and sarcoma genesis. *Clinical Sarcoma Research*. (3)10, (2013).

[80] Stolzing, A., Coleman, N., Scutt, A. Glucose-induced replicative senescence in mesenchymal stem cells. Rejuvenation Res. 9(1), 31-5 (2006).

[81] Bertram, C. and Hass, R. Cellular responses to ROS-induced DNA damage and aging. *Biol Chem.* 389, 211-220 (2008).

[82] Le Blanc, K., Tammik, C., Rosendhal, K., Zetterberg, E., Ringdén, O. HLA expression and immunologic properties of differentiated and undifferentiated mesenchymal stem cells. *PlumX Metrics.* (31)10, 890-896 (2003).

[83] Li, J., Ezzelarab, MB., Cooper, DKC., (2012). Do mesenchymal stem cells function across species barriers? Relevance for xenotransplantation. *Xenotranplantation.* China 19,273-285 (2012).

[84] Hossain, MA., Chowdhury, T., Bagul, A. Imaging modalities for the in vivo surveillance of mesenchymal stromal cells. *J Tissue Eng Regen Med*. 9, 1217–1224 (2015).

[85] Nguyen, PK., Lan, F., Wang, Y., Wu, JC. Guiding the clinical translation of cardiac stem cell therapy. *Circ Res*. 2011, 109:962-979 (2011).

[86] Eggenhofer, E., Luk, F., Dahlke, MH., Hoogduijn, MJ. The life and fate of mesenchymal stem cells. Front Immunol. 19(5), 148 (2014).

[87] Taira, M. Tracking GFP-labeled transplanted mouse MSC in nude mice using in vivo fluorescence imaging. *Nano Biomedicine.* 6(2), (2014).

[88] Fisher, UM., Harting, MT., Jimenez, F., Monzon-Posadas, WO., Xue, H., Savitz, SI. et al. Pulmonary passage is a major obstacle for intravenous stem cell delivery: the pulmonary first pass-effect. *Stem Cells Dev.* 18(5), 683-92 (2009).

[89] Meibohm, B. and Derendorf, H. Basic concepts of pharmacokinetic/pharmacodynamic (PK/PD) modelling. *Int J Clin Pharmacol Ther*. 35(10), 401-413 (1997).

[90] Breimer, DD. and Danhof, M. The relevance of PK-PD modeling in drug development: the wooden shoe paradigm. *Clin Pharmacokin.* 32, 259-67 (1997).

[91] Karp, JM. and Leng Teo, GS. Mesenchymal stem cell homing: the devil is in the details. *Cell Stem Cell.* 4(3), 206-216 (2009).

[92] Kean, TJ., Lin, P., Caplan, A. L., Dennis, J. E. MSCs: delivery routes and engraftment, cell-targeting strategies, and immune modulation. *Stem cells Int.* 2013, 732742 (2013).

[93] Chamberlain, G., Fox J., Ashton, B., Middleton J. Concise review: mesenchymal stem cells: their phenotype, differentiation capacity, immunological features, and potential for homing. *Stem Cells.* 25, 2379-2749 (2007).

[94] Czarnik, AW. and Mei, HY. Comprehensive Medicinal Chemistry. *Elsevier II*. 2, 289-557 (2007).

[95] Zhuang, X. and Lu, C. PBPK modeling and simulation in drug research and development. *Acta Pharmaceutica Sinica*. 6(5), 430–440 (2016).

[96] Physiologically Based Pharmacokinetic Analyses — Format and Content Guidance for Industry. Draft guidance (2016). U.S. Department of Health and Human Services Food and Drug Administration Center for Drug Evaluation and Research (CDER). Clinical Pharmacology. Draft guidance (2016).

[97] Danhof, M., de Jongh, J., De Lange, EC., Della Pasqua, O., Ploeger, BA., Voskuyl. RA. Mechanism-based pharmacokinetic-pharmacodynamic modeling: biophase distribution, receptor theory, and dynamical systems analysis. *Annu Rev Pharmacol Toxicol*. 47, 357-400 (2007).

[98] Gabrielsson, J., Weiner, D. Pharmacokinetic and pharmacodynamic. Data Analysis: Concepts and applications. Apotekarsocieteten (2010).

[99] Bader, P., Kuçi, Z., Bakhtiar, S., Basu O., Bug, G., Dennis, M., et al. Effective treatment of steroid and therapy-refractory acute graft-versus-host disease with a novel mesenchymal stromal cell product (MSC-FFM). *Bone Marrow Transplant*. 53(7), 852-862 (2018).

[100] Kuepfer, L., Niederalt, C., Wendl, T., Schlender, J-F., Willmann, S., Lippert, J. et al. Applied concepts in PBPK Modeling: how to build a PBPK/PD model. *CPT Pharmacometrics Syst Pharmacol.* 5(10), 516–531 (2016).

[101] Zachar, L., Bačenková, D., Rosocha, J. Activation, homing, and role of the mesenchymal stem cells in the inflammatory environment. *J Inflamm Res.* 9, 231–240 (2016).

[102] Murphy, MB., Moncivais, K., Caplan, A. Mesenchymal stem cells: environmentally responsive therapeutics for regenerative medicine. *Exp Mol Med*. 45(11), e54. (2013).

[103] Bernardo, ME. and Fibbe, WF. Mesenchymal Stromal Cells: Sensors and Switchers of Inflammation. *Cell Stem Cell.* 13(4), 392-402 (2013).

[104] Gozzi, P., Påhlman, I., Palmér, L., Grönberg, A., Persson, S. Pharmacokinetic-pharmacokynamic modeling of the immunomodulating agent Susalimod and experimentally induced tumor necrosis factor-α levels in the mouse. *J. Pharmacol. Exp. Ther*. (291)1, 199-203 (1999).

[105] Gabrielsson, J., Hjorth, S., Vogg, B; Harlfinger, S., Morentin Gutierrez, P., Peletier, L. et al. Modelig and design of challenge tests: inflammatory and metabolic biomarker study examples. *Eur J Pharm Sci J.* (67), 144-159 (2015).

[106] Brady, R., Frank-Ito, D. O., Tran, H. T., Janum, S., M, Møller, K., Brix, S., et al. Personalized mathematical model predicting endotoxin-induced inflammatory responses in young men.

[107] Boregowda, S. V., Krishnappa, V., Phinney, G. Isolation of mouse bone marrow mesenchymal stem cells. *Mesenchymal stem cells: methods and protocols.* 1416 (11), 205-223 (2016).

[108] Sepulveda, J, C., Tomé, M., Férnandez, M. E., Delgado, M., Campisi, J., Bernand, A. et al. Cell senescence abrogates the therapeutic potential of human mesenchymal stem cells in the lethal endotoxemia model. *Stem Cells*. (32), 1865-1877 (2014).

[109] Baustian, C., Hanley, S. and Ceredig, R. Isolation, selection and culture methods to enhance clonogenicity of mouse bone marrow derived mesenchymal stromal cell precursors. *Stem Cell Research & Therapy*. 6(151). (2015)

[110] De Barros, J-P. P., Gautier, T., Sali, W., Adrie, C., Choubley, H., Charron, E. Quantitative lipopolysaccharide analysis using HPLC/MS/MS and its combination with the limulus amebocyte lysate assay. *J. Lipid Res.* 56, 1365-1369 (2015).

[111] Shim, G., Lee, S., Han, J., Kim, G., Jin, H., Mao, W. et al. Pharmacokinetics and in vivo fate of intra-articularly transplanted human bone marrow-derived clonal mesenchymal stem cells. *Stem Cells Dev*. 24(9), (2014).

[112] Friedenstein, AJ., Piatetzky-Shapiro, II., Petrakova, K. V. Osteogenesis in transplants of bone marrow cells. *J. Embroyl. Exp. Morph*. 16(3), 381-390 (1966).

[113] Brooks, A., Futrega, K., Liang, X., Hu, X., Liu, X., Crawford, DHG. et al. Concise review: quantitative detection and modeling the in vivo kinetics of therapeutic mesenchymal stem/stromal cells. Stem Cells TM. 7,78-86 (2018).

[114] Cuende, N., Rasko, JEJ., Koh, MBC., Dominici, M., Ikonomou, L. Cell tissue and gene products with marketing authorization in 2018 worldwide. *Cytotherapy* 1-13 (2018).

[115] The Food and Drug Administration for Biologics Evaluation and research Guidance for Industry: preclinical assessment of investigational cellular and gene therapy products. (2013).

[116] Golpanian, S., Schulman, I. H., Ebert, R. F., Heldman, A. W., DiFede, D. L., Yang, P. C. et al. Concise review: review and perspective of cell dosage and routes of administration from preclinical and clinical studies of stem cell therapy for heart disease. *Stem Cell Transl Med*. (5) 186-191 (2016).

[117] Sager, JE., Yu, J., Ragueneau-Majlessi, I., Isoherranen, N. Physiologically based pharmacokinetic (PBPK) modeling and simulation approaches: a systematic review of published models, applications, and model verification. *Drug Metab Dispos.* 43(11), 1823–1837 (2015).

[118] Salvadori, M., Cesari, N., Murgia, A., Puccini, P., Riccardi, B., Dominici, M. Dissecting the Pharmacodynamics and Pharmacokinetics of MSCs to overcome limitations in their clinical translation. *Mol Ther Methods Clin Dev.* 14 (2019).

[119] Wang, H., Liang, X., Xu, Z. P., Crawfard, D. H. G., Liu, X., Robert, M. S. A physiologically based kinetic model for elucidating the in vivo biodistribution of administered mesenchymal stem cells. *Nature.* (2016).

[120] Miao, C., Jiang, X., He, K., Li, P., Liu, Z., Cao, D., Bone marrow stromal cells attenuate LPS-induced mouse acute liver injury via the prostaglandin E2-dependent repression of the NLRP3 inflammasome in Kupffer cells. *Immunology Letters*. 179, 102-113 (2016).

[121] Eliopoulos, A. G., Dumitru, C. C., Wang, C-C., Cho, J., Tsichlis, P. N. Induction of COX-2 by LPS in macrophages is regulated by Tpl2-dependent CREB activation signals. *The EMBO Journal*. 21(18), 4831-4840 (2002).

[122] Hao, K., Qi, Q., Hao, H., Wang, G., Chen Y., Liang, Y. et al. The Pharmacokinetic-pharmacodynamic model of azithromycin for lipopolysaccharide-induced depressive-like behavior in mice. PLoS One. 8(1): e54981 (2013).

[123] Lipopolysaccharide (LPS)-induced macrophage activation and signal transduction in the absence of Src-family kinases Hck, Fgr, and Lyn. *J Exp Med.* 185(9), 1661-1670 (1997).

[124] Sokol, C. L. and Luster, A. D. The chemokine system in innate immunity. Cold Spring Harbor Perspect Biol. 7:a016303 (2015).

[125] Fitzgerald, K. A. and Callard, R. E. Interleukin-13 (IL-13) is a 12-kDa cytokine that is expressed by CD4 T helper 2 (Th2) cells, basophils, eosinophils, mast cells, invariant natural killer T cells, and type 2 innate lymphoid cells. Translational Immunotherapy of Brain Tumors, (2017).

[126] Janeway, CA. Jr., Travers, P., Walport, M., et al. Principles of innate and adaptive immunity. Immunobiology: The Immune System in Health and Disease. 5th edition (2001).